Phase-separated droplets can direct the kinetics of chemical reactions including polymerization, self-replication and oscillating networks

Iris B. A. Smokers[‡[a]], Brent S. Visser[‡[a]], Wojciech P. Lipiński[[a]], Karina K. Nakashima[[a],[b]] and Evan Spruijt*[[a]]

[a] Institute for Molecules and Materials, Radboud University, Heyendaalseweg 135, 6523 AJ Nijmegen, The Netherlands

[b] Current address: Institut de Science et d'Ingénierie Supramoléculaires (ISIS), CNRS UMR 7006, Université de Strasbourg, 8 Allée Gaspard Monge, Strasbourg 67000, France

‡ These authors contributed equally. * Corresponding author, e-mail: e.spruijt@science.ru.nl

Keywords: biocondensates, coacervate protocells, compartmentalization, reaction kinetics, catalysis

Abstract

Phase-separated compartments can localize (bio)chemical reactions and influence their kinetics. They are believed to play an important role both in extant life in the form of biomolecular condensates and at the origins of life as coacervate protocells. However, experimentally testing the influence of coacervates on different reactions is challenging and time-consuming. We therefore use a numerical model to explore the effect of phase-separated droplets on the kinetics and outcome of different chemical reaction systems, where we vary the coacervate volume and partitioning of reactants. We find that the rate of bimolecular reactions has an optimal dilute/coacervate phase volume ratio for a given reactant partitioning. Furthermore, coacervates can accelerate polymerization and self-replication reactions and lead to formation of longer polymers. Lastly, we find that coacervates can 'rescue' oscillating reaction networks in concentration regimes where sustained oscillations do not occur in a single-phase system. Our results indicate that coacervates can direct the outcome of a wide range of reactions and impact fundamental aspects such as yield, reaction pathway selection, product length and emergent functions. This may have far-reaching implications for origins of life, synthetic cells and the fate and function of biological condensates.

Introduction

It is hypothesized that phase-separated droplets called coacervates play important roles both in extant life and at the origins of life.[1–3] Cellular coacervates are commonly called membraneless organelles or biomolecular condensates and they include the nucleolus, stress granules and Cajal bodies.[4] Their functions in health include cellular organization, signaling and RNA processing, but emerging evidence suggests that coacervates also play a role in protein aggregation linking them to neurodegenerative diseases.[5,6] In the origins of life field, coacervates have been proposed as protocells: a first generation of cellular compartments in which processes important to proto-life could be localized.[3,7]

In all these cases, the local physicochemical milieu inside the coacervate or biomolecular condensate offers a distinct environment that can significantly influence (bio)chemical reactions. Guest molecules that have favorable interaction with the coacervate components are locally enriched inside the droplets, while molecules that do not interact are excluded. At equilibrium, a constant ratio of concentrations is maintained between the dense coacervate phase and the dilute surrounding phase, which is governed by the partition coefficient K_P, while at the same time molecules are continuously exchanged between the coacervate and its surroundings. This enhanced local concentration and exchange has been shown to affect the kinetics of reactions in coacervates.[8–16] Additionally, the local polarity, crowding, pH and water activity can have substantial effects on the energy landscape of reactions, affecting both reaction rates and pathways.[17]

A wide range of reactions have been shown to be enhanced by localization to a coacervate, including enzymatic[8,12,14–16,18] and nanoparticle-catalysed[8,19] reactions, ribozyme reactions,[13,20–22] reactions between synthetic and prebiotically-relevant small molecules,[9–11,23,24] template-directed RNA polymerization,[25] DNA ligation[26] and cell-free gene expression.[27] Our group has recently also shown that coacervates can lead to preferential formation of specific products in peptide ligation by oxidative coupling of α-amidothioacids and amino acids,[24] showcasing that coacervates can not only accelerate reactions, but also direct reaction pathways. We hypothesize that coacervates can have significant and non-trivial effects on a range of reaction types and in reaction networks. However, experimentally testing these effects is challenging and time-consuming. Computer model predictions may provide a solution to identify interesting reaction types and elucidate design principles for desired reaction outcomes, and can serve as a guide for experiments. Previous theoretical work has provided

fundamental insights into processes such as protein aggregation,[28,29] heterodimerization and cluster formation,[30] and enzymatic activity in coacervates,[31] but a versatile and easily adaptable model for practical chemical reactions and reaction networks that is able to explain how experimental systems can be optimized to get a desired reaction outcome, is still lacking.

In this work we use a numerical model to investigate how coacervates can affect the kinetics of reactions that are relevant for (the emergence of) life, based on changes in the partition coefficient of reagents and products, local changes in rate constant and exchange between the dense and dilute phase. We find that the rate of elementary reactions in coacervates can be optimized by tuning the partition coefficient and volume ratio between the dilute and coacervate phase. Polymerization and self-replication reactions can be accelerated in a two-phase system, and coacervates can favor the formation of longer polymers, while locally improving polydispersity, possibly allowing for better information storage in coacervate protocells. Lastly, we find that for oscillating reaction networks the periodicity and amplitude of oscillations can be altered by incorporation in a two-phase system, and oscillations can even be 'rescued' in concentration regimes where sustained oscillations do not take place in a single-phase system.

Methods

In all systems presented in this paper we assume that reactions occur in a two-phase system, composed of two compartments representing the dilute phase and the dense phase of a physical phase-separated system. We consider reactants and products to be dilute guest molecules that are not involved in phase separation and that exhibit ideal solution behavior. We assume that the reactants do not change the volume, viscosity, density or polarity of the dense phase upon partitioning, so their reaction rate constants in both phases are not affected by partitioning. For cases where reactants or products are directly involved in phase separation, ideal behavior can no longer be assumed, and we refer to a recent article by Bauermann et al who showed how chemical and phase equilibria are linked in such cases.[32]

We assume that all reactions can occur in both phases and that the reactants and products are transported between the phases. Partition coefficients ($\frac{k_{\mathrm{dil}\rightarrow\mathrm{cond}}}{k_{\mathrm{cond}\rightarrow\mathrm{dil}}} = \frac{c_{\mathrm{cond}}}{c_{\mathrm{dil}}} = K_{\mathrm{P}}$) are determined by the ratio of the transport rate from the dilute phase into the dense phase and the transport rate

from the dense phase to the dilute phase, which is equal to the ratio of the concentration in the dense and dilute phase. In all simulations the ratio of volumes of the dilute phase to the dense phase is fixed and described by parameter $R = \frac{V_{\mathrm{dil}}}{V_{\mathrm{cond}}}$. For instance, $R = 100$ means that the volume of the dense phase is 100-times smaller than the volume of the dilute phase. We also note that the volume fraction of the dense phase ϕ is inversely related to R via $\phi = 1/(1 + R)$.

All reactions and the transport equations compose a set of differential equations that are solved numerically to obtain the concentration of reactants over time (per phase). For example, for the first order reaction ($A \rightarrow B$) we use the following set of equations:

$$\frac{d[A]_{\mathrm{dil}}}{dt} = k[A]_{\mathrm{dil}} - k_{\mathrm{dil}\rightarrow\mathrm{cond}}[A]_{\mathrm{dil}} + k_{\mathrm{cond}\rightarrow\mathrm{dil}}[A]_{\mathrm{cond}}$$

$$\frac{d[A]_{\mathrm{cond}}}{dt} = k[A]_{\mathrm{cond}} + Rk_{\mathrm{dil}\rightarrow\mathrm{cond}}[A]_{\mathrm{dil}} - Rk_{\mathrm{cond}\rightarrow\mathrm{dil}}[A]_{\mathrm{cond}}$$

The inclusion of R in the transport equation for the dense phase ensures that transporting one unit of concentration of reactant from the dilute phase to the dense phase produces R units of concentration in the dense phase (due to R-times smaller volume).

Systems of differential equations for more complex reactions are constructed analogously. Below we present the schematic representations of the reaction systems studied and we provide the full description of the corresponding systems of differential equations in Supplementary Information Section 1.

Results and discussion

Rate acceleration is optimal for $R = K_P$

To establish the foundations of chemical reaction kinetics in phase-separated droplets, we investigate a simple bimolecular reaction A + B → C in coacervates (Figure 1a), inspired by the aldol reactions and hydrazone formation reactions that have been reported in the presence of simple and complex coacervates.[9,10] For simplicity, we assume that the rate constant k is not affected by the coacervate environment, and focus on the effect of local accumulation of reagents inside the coacervates. Although Bauermann et al recently showed that at phase equilibrium reaction rates for coacervate-forming (scaffold) molecules are solely determined by a change in *k*, because their chemical potential,

and thus, activity is equal between the phases, this does not hold for the dilute guest molecules we consider here, as they do not contribute to phase separation. For dilute guests, the local concentration is therefore an important contributor to the reaction rate. This situation is reminiscent of the enhanced reactivity of hydrophobic compounds in micellar catalysis.[33]

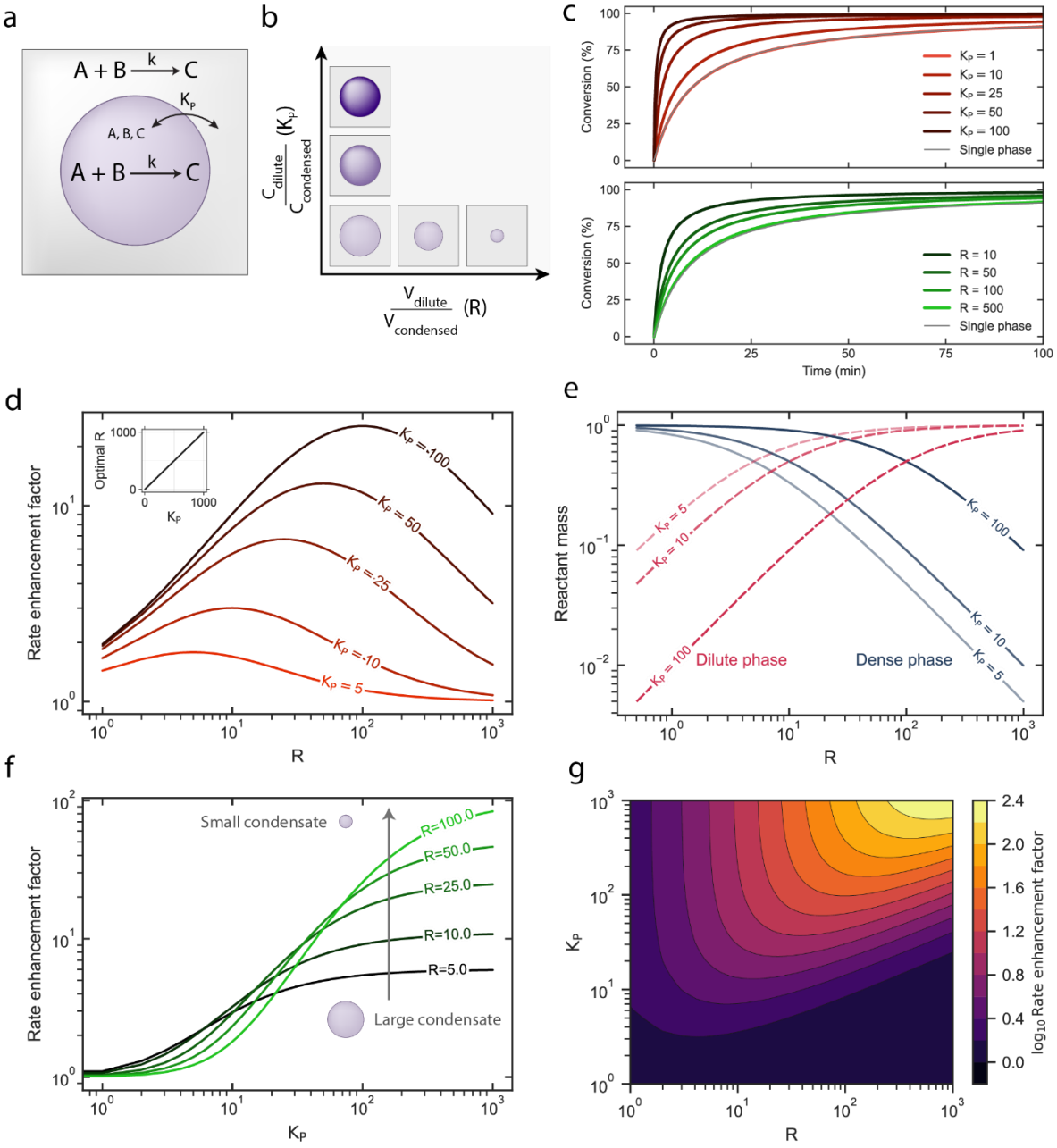

Figure 1. Bimolecular reaction system in two phases. (a) A bimolecular reaction A + B → C is modeled in two phases with an identical rate constant in both phases. All molecules can travel freely between both phases. **(b)** We vary the partition coefficient (K_P) and volume ratio (R) in our simulations. **(c)** Top: Higher partitioning of the components speeds up the reaction (R = 100). Bottom: Reaction rate converges to rate in single phase for very small coacervate volumes (K_P = 10). **(d)** For a set K_P, the relative rate enhancement ($k_{\text{two phase}}$ / $k_{\text{single phase}}$) of the simple reaction in a two-phase system is optimal when R is equal to the K_P. Inset shows the R at which rate enhancement is maximum versus K_P. **(e)** The rate enhancement of the reaction is always higher for a higher value of K_P, regardless of R. Larger compartments enhance the reaction more for smaller K_P, while smaller compartments have a larger increase for a higher K_P. **(f)** At $R = K_P$ the dense and dilute phase contain an equal amount of reactant. **(g)** Heatmap of the overall rate enhancement for the full range of R and K_P.

We vary K_{P} between 1 – 1000 and R between 1 – 1000 (i.e. from having 50% v/v to ~0.1% v/v dense phase), ranges that are achievable in experimental systems (Figure 1b). For simplicity, K_{P}'s of all components are equal, unless otherwise specified. Experimental partition coefficients are often in the range of 2 to 50,[9,10,34] but values as high as K_{P} = 10,000 have been reported.[35,36] The range of R in experimental systems can vary widely depending on the coacervate-forming components and the location in the phase diagram. For biomolecule-based coacervates, R is often in the range of 200 – 2000,[36] although R can become infinitely large at the edge of the phase diagram ($R \to \infty$ when $\phi \to 0$). On the other hand, for coacervates prepared with synthetic polymers (for which larger monomer concentrations can be obtained), values of R lower than 1 have been observed.[37]

First, we simulated how the partition coefficient K_P of the reactants affects the overall reaction time, with fixed R = 100. As expected, we find that higher partitioning leads to a faster reaction (Figure 1c). This simple example shows the potential of even relatively small amounts of coacervate phase to have a substantial effect on the overall reaction rate of the bulk. In the case of varying the phase volume ratio R (at fixed K_P= 10), we observe highest rate enhancement for R = 10 with the reaction rate converging to the rate in a single phase for large values of R (Figure 1c), i.e. for a smaller volume of coacervate phase. This is to be expected, as for a smaller coacervate phase volume at constant partitioning, the relative contribution of the dense phase reaction to the overall reaction diminishes.

The observed rate enhancement by coacervates led us to investigate the relationship between R and K_P, by calculating the apparent overall rate constant based on the change in the total concentration of C ($k_{\text{two phase}}$). We normalized these apparent rate constants by dividing them by the rate constant of the single-phase reaction, given by rate constant $k_{\text{single phase}}$. We first analyzed how changing R at different, constant values of K_P changes the apparent rate constant of the entire system. We found that for any value of K_P there is an optimal value of R to achieve the highest rate enhancement (Figure 1d). Such a maximum was recently also observed by Laha et al.[30] Further analysis showed that the peak coincides with $R = K_P$, which we also find by analytically examining our system (Supplementary Information Section 2.1). This can be understood by considering that the optimal rate enhancement is related to the total amount of material within the coacervates and the local concentration. At $R = K_P$, the amount of reactant in the dense and dilute phase is equal (Figure 1e).

Because the total amount of reactant is fixed, a decrease in R will result in a lower reactant concentration inside the dense phase (Supplementary Information Figure 3), and thereby lead to a lower local reaction rate inside the coacervates, while an increase in R will lower the amount of reactant in the dense phase (Figure 1e) and thereby reduce the effect of the dense phase reaction on the overall reaction rate. Further examination also showed that when the rate constant k is locally different inside the coacervate, the maximum rate enhancement is still approximately at $R = K_P$, even for a ten-fold increase in rate constant (Supplementary Information Section 2.1, Supplementary Figure 2).

On the other hand, when we varied K_P for a set of constant R values, we found that for any R, the highest rate can be achieved by increasing the K_P (Figure 1f). This observation can be rationalized by the fact that concentrating a larger number of molecules into a smaller compartment consistently results in a faster reaction. Interestingly, for smaller values of R rate enhancement is already observed for lower partitioning, but the maximum rate enhancement is limited due to the larger compartment. Smaller compartments show the potential to achieve higher overall rate enhancements, provided there is a sufficiently large K_P.

Taken together, these results highlight that rates are always highest when the reactants are concentrated as much as possible (i.e. high K_P), under the assumption that ideal solution behavior is retained, but for a given K_P, there is an optimal ratio of volumes for the two phases to achieve the highest rate enhancement (Figure 1g). We expect that in experimental and biological systems there is often partial control over the ratio of the two phases by controlling the concentration of the phase separating material, but there is limited control over the partitioning of the reactants. Although molecules could be functionalized with groups that enhance their partitioning, such modifications will often also affect their reactivity, especially in the case of small molecules. We show here that for such cases, tuning the volume ratio of the coacervate phase versus the dilute phase is a helpful method to control the reaction rate.

Coacervates promote longer sequences in polymerization reactions

Inspired by these results for a simple bimolecular reaction, we wondered what effects coacervates could exert on more complex reactions and networks. We first investigated a polymerization reaction

in coacervates. In addition to having industrial relevance,[38–40] optimization of polymerization reactions by coacervates can give important insights for the origins of life: formation of the first biopolymers (RNA, DNA, peptides) is thought to be crucial for the emergence of life.[41,42] It is known that polymerization can be aided by minerals[43] or by drying the reaction mixture down to a paste,[44–46] as both these processes locally increase the concentration of reagents. Coacervates can similarly increase reagent concentration, but a systematic analysis of their effect on polymerization reactions is lacking.

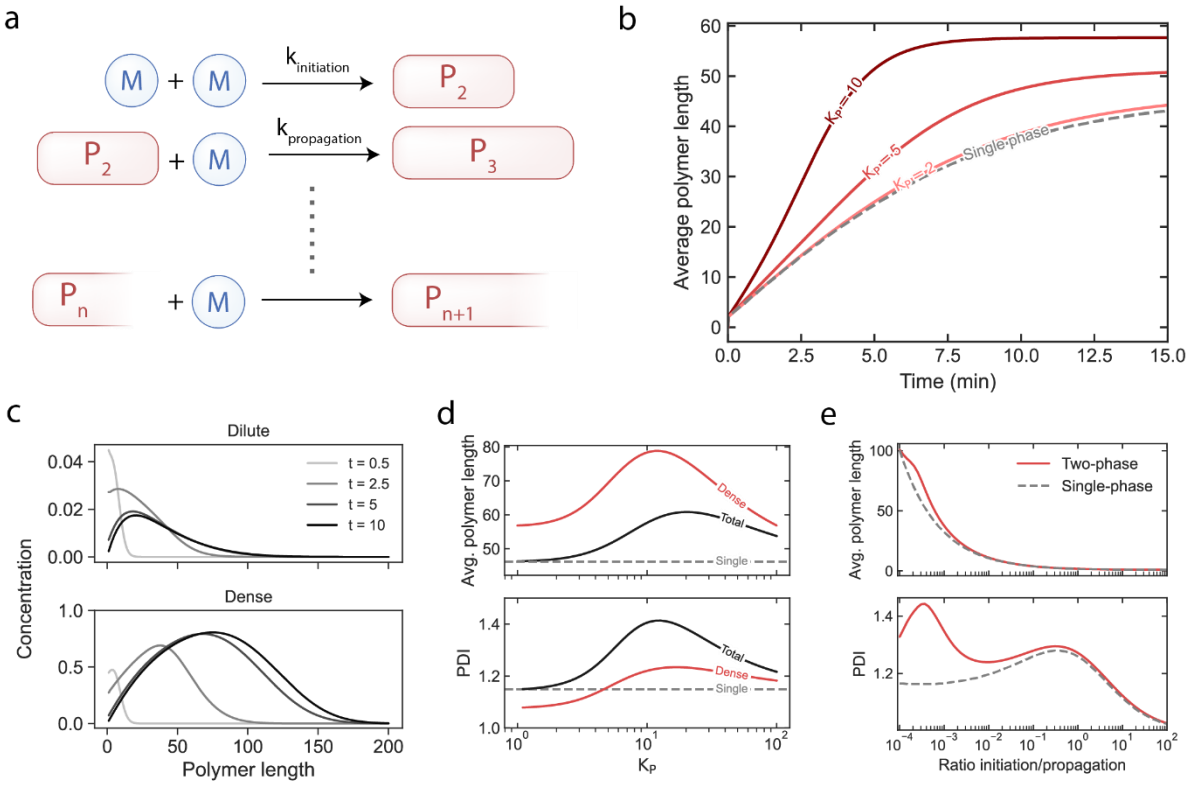

Figure 2. Polymerization in two phases. (a) Schematic overview of the chain growth polymerization reaction that can occur in two phases. Longer polymers have a lower transfer rate out of the coacervate, and therefore a higher K_P. **(b)** Increased partitioning leads to a faster formation of longer polymers and higher final average polymer length. K_P is defined as the K_P of the monomer (R = 100). **(c)** The dilute (top) and dense phase (bottom) have a distinct distribution of polymer lengths over the course of the reaction, with the dense phase retaining longer polymers ($K_{P,monomer}$ = 10; R = 100). **(d)** Top: The number average final polymer length increases for stronger partitioning up to a maximum around K_P = 20 for the total sample and K_P = 12 for the dense phase. The final polymer length is consistently longer than for a single-phase system. Bottom: The obtained polydispersity index (PDI) follows a similar trend as the final average polymer length, with a maximum around K_P = 10 for the total sample and K_P = 15 for the dense phase. **(e)** The obtained average polymer length and PDI vary as a function of the ratio of the initiation and propagation rate, with a pronounced difference between a single-phase and two-phase system for slow initiation compared to propagation ($K_{P,monomer}$ = 10; R = 100).

To determine the effects of coacervates on the chain length and polydispersity of the polymerization products, we investigated a chain growth polymerization reaction (Figure 2a), of which both the monomers and products partition into the coacervate. Because longer polymers have a

stronger interaction with the coacervate matrix and have slower dynamics,[47,48] we modelled the longer polymers to have a lower $k_{\mathrm{cond}\rightarrow\mathrm{dil}}$ following an exponential decay and concomitant higher K_P (Supplementary Figure 6). We further assumed that all polymer lengths have equal $k_{\mathrm{propagation}}$, and the polymerization to be living, i.e. to not terminate.

First, we modelled how the number average polymer length is affected by partitioning into coacervates compared to a single-phase reaction (Figure 2b, d). This was done by simulating the concentration of all polymeric species (up to a cutoff length n = 200). We confirmed that the cut-off length does not influence the output of our model: at the end of the reaction the concentrations of length 200 are below $1{\cdot}10^{-12}$ (Supplementary Figure 7-8, Supplementary Movie 1). We find that by increasing the partitioning of the reactants (K_P is the partition coefficient of the monomer), the reaction rate increases and long polymers are formed faster than in a single-phase reaction. Additionally, the final average polymer length is increased, up to a maximum for K_P = 20 (Figure 2.d. top). For K_P > 20 the average polymer length was found to decrease. Under these conditions, both the initiation and propagation take place almost exclusively in the dense phase (Supplementary Figure 9), and inside the dense phase the contribution of the initiation reaction increases (Supplementary Figure 10), most likely because of an increasingly high local concentration of monomers which has a comparatively larger effect on initiation (which is second-order in monomer) than on propagation (which is first-order in monomer). The maximum in polymer length as a function of K_P is directly related to the contributions of initiation and propagation to the total system, for which the minimum in contribution of initiation coincides with the maximum in average polymer length (Supplementary Figure 10). Changes in R also affect the average final polymer length, with larger R giving the largest final polymer length, while intermediate R gives a faster formation of long polymers (Supplementary Figure 12).

The increase in average polymer length is accompanied by a broadening of the distribution of polymer lengths (Supplementary Figure 8, Supplementary Movie 1), as the dense phase retains the long polymer sequences, while the dilute phase is enriched in shorter sequences (Figure 2c). This results in a higher polydispersity index (PDI) for moderate K_P's than for low K_P (Figure 2d bottom). For larger K_P's, however, the PDI decreases again following the decrease in average polymer length. The polydispersity in a single-phase system is, however, always lower than in a two-phase system.

Nevertheless, for low to intermediate K_P the local PDI of all polymers in the dense phase is lower than the PDI of all polymers formed in a single-phase system, while a higher average polymer length is obtained. This suggests that coacervates may serve to select polymers based on length, and reduce the local variations in length. Isolation of the dense phase after the polymerization reaction is completed may yield long polymers with a low polydispersity.

To generalize our model for polymerization reactions with different rates, we modulated the ratio between the rate of initiation and propagation. We analyzed the average polymer length at the end of the reaction (Figure 2e) for both a two-phase and a single-phase system. Only for slow initiation compared to propagation (low ratio) a difference is observed between a two-phase and single-phase system, with the reaction in a two-phase system leading to a larger final polymer length. For faster initiation, more polymers are nucleated and the final polymer length is shorter due to the limited amount of monomer. Under these conditions, coacervates do not make a significant difference to the final polymer length that is obtained, because due the shorter final length, the effect of retention of longer sequences in the coacervate is less strong. Also, the difference in PDI is larger for slow initiation and diminishes for fast initiation, although for the PDI the difference between a two-phase and single-phase system remains up to higher ratios of initiation to propagation.

These results show that coacervates are a promising environment for forming longer polymers. Isolation of the dense phase after completion of the reaction could yield long polymers with low PDI and might be useful for industrial purposes. For the origins of life we would argue that the importance of forming longer sequences outweighs the disadvantage of having a larger PDI in the total two-phase system. The formation of longer polymers would make it possible to store more information in the first genetic polymers and these longer sequences could be selectively retained inside coacervate protocells. Longer sequences of RNA are also more likely to gain catalytic function. Similarly, longer peptide sequences are more likely to have a defined fold or undergo phase separation, which would allow the coacervate to promote the formation of its own material. Lastly, a larger population of long polymers can cover a larger sequence space, increasing the chance of creating functional sequences.

Self-replication rate can be increased in coacervates

To replicate the sequence information stored in prebiotic biopolymers, self-replication is thought to have preceded more complex enzyme-based replication.[49,50] Self-replicating DNAs,[51,52] peptides,[53,54] ribozymes[55–57] and synthetic molecules[58,59] have been developed, which replicate themselves by coordination of two building blocks to a template, which increases the effective molarity of the building blocks and facilitates their ligation, forming a copy of the template molecule (Figure 3a). A general problem in most of these systems, however, is product inhibition: dissociation of the formed template duplex is so slow that it prevents the product template from catalyzing a new round of replication.[49] Coacervates have been shown to melt nucleic acid duplexes,[60,61] and could therefore potentially alleviate product inhibition. This is a delicate balance, as the same interactions that weaken the template duplex are also likely to weaken the interaction between template and building blocks.[3] Another step in the replication process that coacervates can affect is the rate of ligation between the building blocks, which can be increased due to a higher local concentration.

The functioning of self-replicators inside coacervate protocells has recently received a lot of attention. Several self-replicating DNA and ribozyme systems have been shown to function inside coacervates,[22,25,62] and in some cases the replication rate is even enhanced.[13] How well self-replication works is highly dependent on the nature of the coacervate material.[25,62] We aimed to get a deeper understanding of how coacervates can promote self-replication and help overcome product inhibition.

We modelled a templated self-replication reaction with two pathways, a non-catalytic pathway in which a bimolecular reaction of A + B forms template T, and a catalytic pathway in which A and B coordinate to T to form a complex [ABT] upon which ligation forms a duplex of templates TT, which are subsequently released (Figure 3a). We assessed if the introduction of the coacervate phase could change the relation of the autocatalytic pathway to the non-autocatalytic pathway. To do so, we integrate the total concentration of T formed through both reactions over time (Figure 3b). For visualization purposes, system parameters were chosen so that cumulative contributions of both reactions are close to equal in the single-phase system, starting with no T present. Under these conditions $\frac{k_{\text{autocatalytic ligation}}}{k_{\text{bimolecular}}} = 16.4$, which is in the lower range of values found for experimental self-replicating systems (Supplementary Table 5).[52,53,55,63] The results for a 100x larger ratio between the

pathways are similar and are described in Supplementary Information Section 4.3. We normalize the total contribution of both pathways to 1 to compare how the relative contributions of both reactions change in a two-phase system with differing K_P of the components (Figure 3c). We assumed that all reaction components partition to the same extent.

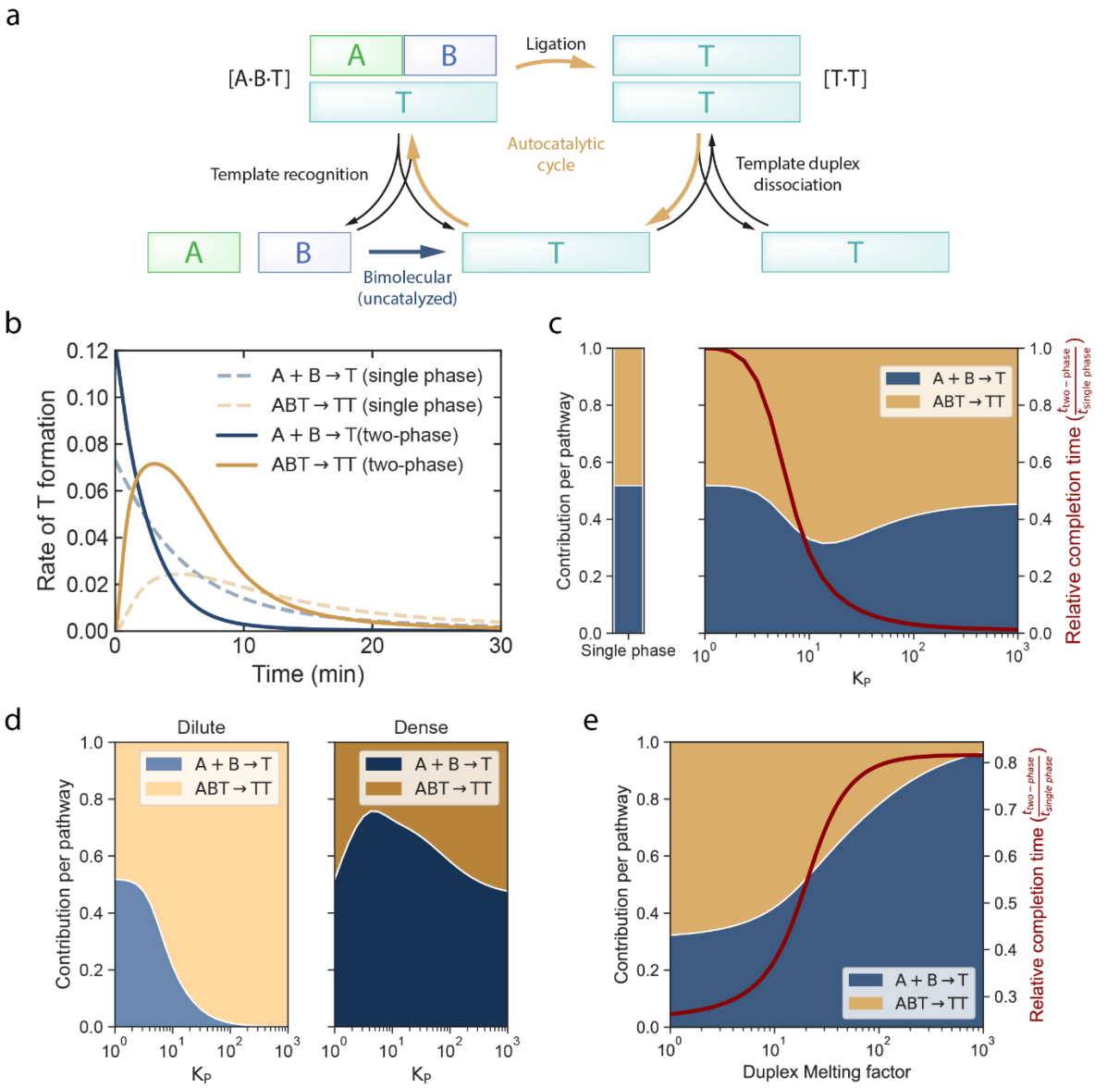

Figure 3. Self-replication in two phases. (a) Schematic overview of the self-replication that can take place in a two-phase system. Building blocks A and B can react in an uncatalyzed bimolecular reaction to form template T, which can then catalyze its own formation by binding the building blocks and aiding their ligation. A common limit in most experimental systems is the slow dissociation of the template duplex to release the template strands for a further round of replication. **(b)** A comparison between the T formed through the autocatalytic (ABT → TT) and non-autocatalytic pathway (A + B → T) in a single phase and in a two-phase system (K_P = 10, R = 100). **(c)** The contribution of the autocatalytic pathway has a maximum around K_P = 10, after which it decreases again for large K_P. The completion time for the reaction (normalized to the completion time in a single-phase system) decreases as a function of K_P. K_P is kept equal for all components in the system. **(d)** In the dilute phase, an increased K_P leads to nearly exclusively autocatalytic formation of T. In the dense phase, the non-autocatalytic pathway reaches a maximum around K_P = 5, after which it decreases to an equal contribution of both pathways at large K_P. **(e)** Duplex melting within the dense phase leads to an increase in the non-autocatalytic pathway, while increasing the completion time for the reaction (K_P = 10, R = 100).

In the case of equal partitioning between the condensate and coexisting dilute phase (K_P = 1), no change in the relative contributions is found compared to a single-phase system, as expected. However, we find that beyond K_P = 1, there is an optimum in the relative contribution of the autocatalytic reaction to the self-replication at intermediate K_P. For higher partitioning the formation of T occurs faster, while the contribution of the autocatalytic pathway decreases again (Figure 3c). When we divide the contributions between the two phases, we can see that in the dilute phase the reaction is increasingly autocatalytic for higher K_P (Figure 3d). The dense phase, on the other hand, starts with equal contribution of both pathways for K_P = 1, but shows a strong increase in contribution from the bimolecular pathway until a maximum is reached at K_P = 5, after which its contribution decreases again. For low K_P (up to K_P = 10) the reaction in the dilute phase has the largest effect on the overall distribution of pathways in Figure 3c. However, for larger K_P (K_P > 30), the reaction in the dense phase starts to determine the overall reactions (Supplementary Figure 15), as under these conditions the majority of the reactant mass is in the dense phase and the majority of T is formed there. By inhibiting transfer between the phases for individual components (Supplementary Figure 16-22), we were able to find that transfer of ABT from the dense to the dilute phase is critical to obtain the contributions in Figure 3c. Formation of ABT is the most unfavorable step, as it is the step with the highest molecularity. The high concentration in the dense phase favors ABT formation (Supplementary Figure 23-24), after which it is rapidly transferred to the dilute phase, where it reacts to form TT (Supplementary Figure 25). These observations show that free transfer between the phases is crucial for the functioning of the self-replication reaction in a two-phase system. Although a concentration-dependent distribution of the pathways is also observed in a single phase, the maximum contribution of the autocatalytic pathway is slightly larger in the two-phase system (0.3 vs. 0.4), and, most importantly, the completion time for the reaction can be significantly reduced in a two-phase system (Figure 3c), without having to increase the overall reagent concentration.

To investigate the effect of coacervates on product inhibition, we modulated the strength of complex formation between T + T ↔ TT and A + B + T ↔ ABT by introducing a 'duplex melting factor' that increases the dissociation constant for both equilibria to the same extent. In experimental systems, such an increase in dissociation constant could be obtained by changing the charge-density, charge-type, length and charge-balance of the coacervate components,[21,25,62,64] or by the extent of

Mg^{2+} partitioning for ribozyme self-replicators.[62] Increasing the duplex melting factor increases the contribution of the bimolecular pathway (Figure 3e), and increases the relative completion time. It is therefore unlikely that coacervates will alleviate product inhibition, especially considering that in experimental systems the termolecular ABT complex is likely weakened more than the bimolecular TT complex.

Although reduction of product inhibition cannot be achieved with coacervates – and must instead be achieved by structurally changing the reactants or by temporal changes in the dissociation constant – coacervates can aid self-replication reactions by accelerating the reaction through local accumulation of reagents, making it more likely for self-replication to take place in the dilute conditions on prebiotic Earth.

Coacervates can alter the periodicity and robustness of oscillating chemical reaction networks

Lastly, we investigated how coacervates can affect more complex reaction networks, such as networks that display oscillatory behavior. Oscillatory behavior can emerge in out-of-equilibrium systems and is known to drive many processes important to life, such as circadian rhythm and the cell-cycle.[65,66] Oscillations can only be achieved when a chemical network system is complex enough and there is sufficient delay in the reactions.[67,68] The periodicity, amplitude and persistence of oscillations are dependent on reactant concentrations and rate constants, and could therefore be tuned by the local conditions inside the coacervate phase.

We modelled an oscillating system based on the Brusselator[69–71] (Figure 4a) to investigate what effect K_P, R and the transfer rate between the phases can have on oscillations. We started with varying K_P and observe that stronger partitioning results in a shorter period and lower amplitude of the oscillations (Figure 4b, e, Supplementary Figure 31, Supplementary Movie 2). To determine the period of the oscillations, we found local maxima by comparing neighboring values and calculated the average time between them for oscillations between 5 and 50 minutes. Around K_P = 11, the limit cycle breaks down and the oscillation becomes unstable (Supplementary Movie 2). Similar behavior is observed for a single-phase system at high concentrations (Supplementary Figure 32-33). In addition to K_P, the period and amplitude are also affected by R (Figure 4c-e, Supplementary Figure 31, Supplementary Movie 3). The period does not decrease linearly upon R, but has a steep decline

between R = 25 and R = 35, after which it reaches a minimum around R = 40 and it slowly increases again for larger R. The onset of the steep decline corresponds to the point where the oscillations collapse into a smaller limit cycle and the system undergoes transient instability before entering the limit cycle (Figure 4d, Supplementary Figure 34-35, Supplementary Movie 3). The maximum amplitude, however, does show a gradual decrease for larger R, but similarly increases again for large R.

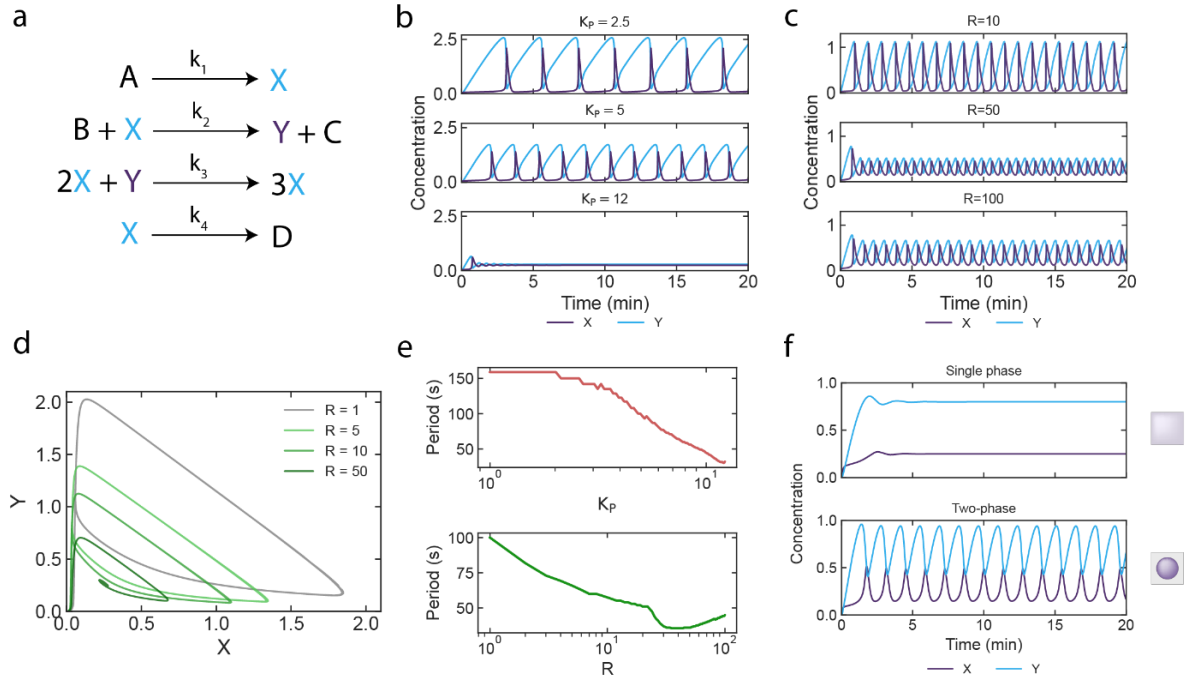

Figure 4. Oscillatory reactions in two phases. (a) Schematic overview of the Brusselator reactions. All reaction components partition equally into the coacervate phase. **(b)** A larger K_P lowers the periodicity and amplitude of the oscillations (R = 100). At K_P = 12 sustained oscillations are no longer observed. **(c)** A larger R lowers the periodicity and amplitude of the oscillations down to a minimum, after which they increase again. **(d)** Phase plot showing the decreased periodicity and amplitude for higher R (K_P = 10). At R = 50, the system undergoes transient instability before entering the limit cycle. **(e)** Average period of oscillations between 5 and 50 minutes of the reaction as a function of K_P (R = 100) and R (K_P = 10). The period decreases as a function of K_P up to K_P = 11. The period of oscillations decreases as a function of R with an increase in slope around R = 25, and a minimum around R = 40, after which the period increases again. **(f)** For different partitioning of reactants, a two-phase system (bottom; $K_{P\,A,C,X,Y}$ = 5, $K_{P\,B}$ = 30, R = 100) can sustain oscillations at overall concentrations that do not give sustained oscillations in a single phase (top).

In addition to giving changes in amplitude and periodicity of oscillations, coacervates can help to sustain oscillations in concentration regimes that do not give sustained oscillations in a single phase because they do not fulfill the criterion [B] < [A]^2 + 1 (Figure 4e top). When B partitions more strongly than A – in this case $K_{P\,A,C,X,Y}$ = 5 and $K_{P\,B}$ = 30 – the concentrations inside the coacervate phase still obey the criterion for sustained oscillations, and stable oscillations are maintained in the system overall. In this way, coacervates can increase the robustness of the oscillatory network.

The changes in period, amplitude and robustness caused by including oscillatory reaction networks in a two-phase system affect the timekeeping and output of the system, and thereby alter its function. Such changes can have profound effects on downstream reactions coupled to the oscillatory network,[72] and could possibly play a role in oscillating biomolecular reaction networks in the cell in presence of biocondensates.

Discussion

In this work, we have shown that coacervates can direct outcomes of several chemical reaction systems. We found that the reaction rate of elementary bimolecular reactions can be significantly increased in coacervates and can be optimized by either increasing the partition coefficient, or by adjusting the phase volume ratio R to equal K_P. These insights allow for optimization of reactions rates in experimental systems by either modifying the reactants to have stronger partitioning or by adjusting the amount of coacervate material to get the desired volume ratio. We further showed that coacervates can cause unexpected outcomes for more complex reactions. For polymerization reactions inclusion in coacervates can lead to faster polymerization and formation of longer polymers. For self-replication the reaction can be significantly accelerated by introduction into a two-phase system, although duplex melting inside the coacervate does not help to alleviate product inhibition. Lastly, coacervates can affect both the periodicity and amplitude of oscillating networks and can even 'rescue' oscillations in concentration regimes where oscillations are not sustained in a single-phase system.

In our model we assumed transfer between the phases to be non-limiting (except for the polymerization reaction), so that a single large coacervate droplet is equivalent to several small droplets. In some experimental systems, however, the interface might form a physical barrier for transport between the coacervate phase and the dilute phase due to the interfacial resistance.[73] This effect is expected to be stronger for larger molecules that can adopt different conformations, of which some do not interact with the coacervate material due to shielding of interacting regions of the sequence, and would therefore 'bounce off' the interface. In such cases a large coacervate surface area (as is obtained for many small droplets) would slow down exchange and a single large coacervate droplet would be more favorable. In the case of diffusion-limited reactions, however, a large interface

area might actually be advantageous, as under these conditions substrate can be supplemented from the dilute phase more rapidly. For such cases, the coacervate surface area (and therefore droplet size) will further influence the kinetics of the system, and may give rise to emergent phenomena such as synchronization.

Taken together, our results show that coacervates hold great promise as microreactors that could direct the outcome of a wide range of reactions, including biochemical reactions in biological condensates, prebiotic reactions at the origins of life and synthetic reactions for industrial purposes.

Supporting Information

Additional simulation results, methods, rate equations and model parameters, analytical derivation of relationship between R and K_P for bimolecular reactions, supplementary movies of phase plots and polymer length distribution (PDF).

Acknowledgements

This project received funding from the European Research Council (ERC) under the European Union's Horizon 2020 research and innovation program under grant agreement number 851963, and a Vidi grant from the Netherlands Organization for Scientific Research (NWO).

References

(1) Yewdall, N. A.; André, A. A. M.; Lu, T.; Spruijt, E. Coacervates as Models of Membraneless Organelles. *Curr. Opin. Colloid Interface Sci.* **2021**, *52*, 101416. https://doi.org/10.1016/j.cocis.2020.101416.

(2) Ghosh, B.; Bose, R.; Tang, T. Y. D. Can Coacervation Unify Disparate Hypotheses in the Origin of Cellular Life? *Curr. Opin. Colloid Interface Sci.* **2021**, *52*, 101415. https://doi.org/10.1016/j.cocis.2020.101415.

(3) Slootbeek, A. D.; van Haren, M. H. I.; Smokers, I. B. A.; Spruijt, E. Growth, Replication and Division Enable Evolution of Coacervate Protocells. *Chem. Commun.* **2022**, *58* (80), 11183–11200. https://doi.org/10.1039/d2cc03541c.

(4) Banani, S. F.; Lee, H. O.; Hyman, A. A.; Rosen, M. K. Biomolecular Condensates: Organizers of Cellular Biochemistry. *Nat. Rev. Mol. Cell Biol.* **2017**, *18* (5), 285–298. https://doi.org/10.1038/nrm.2017.7.

(5) Lipiński, W. P.; Visser, B. S.; Robu, I.; Fakhree, M. A. A.; Lindhoud, S.; Claessens, M. M. A. E.; Spruijt, E. Biomolecular Condensates Can Both Accelerate and Suppress Aggregation of α-Synuclein. *Sci. Adv.* **2022**, *8* (48), 6495. https://doi.org/10.1126/sciadv.abq6495.

(6) Mathieu, C.; Pappu, R. V.; Paul Taylor, J. Beyond Aggregation: Pathological Phase Transitions in Neurodegenerative Disease. *Science* **2020**, *370* (6512).

https://doi.org/10.1126/science.abb8032.
(7) Van Haren, M. H. I.; Nakashima, K. K.; Spruijt, E. Coacervate-Based Protocells: Integration of Life-like Properties in a Droplet. *J. Syst. Chem.* **2020**, *8*, 107–120.
(8) Koga, S.; Williams, D. S.; Perriman, A. W.; Mann, S. Peptide-Nucleotide Microdroplets as a Step towards a Membrane-Free Protocell Model. *Nat. Chem.* **2011**, *3* (9), 720–724. https://doi.org/10.1038/nchem.1110.
(9) Smokers, I. B. A.; van Haren, M. H. I.; Lu, T.; Spruijt, E. Complex Coacervation and Compartmentalized Conversion of Prebiotically Relevant Metabolites**. *ChemSystemsChem* **2022**, *4* (4), e202200004. https://doi.org/10.1002/syst.202200004.
(10) Abbas, M.; Lipiński, W. P.; Nakashima, K. K.; Huck, W. T. S.; Spruijt, E. A Short Peptide Synthon for Liquid–Liquid Phase Separation. *Nat. Chem.* **2021**, *13* (11), 1046–1054. https://doi.org/10.1038/s41557-021-00788-x.
(11) Jacobs, M. I.; Jira, E. R.; Schroeder, C. M. Understanding How Coacervates Drive Reversible Small Molecule Reactions to Promote Molecular Complexity. *Langmuir* **2021**, *37* (49), 14323–14335. https://doi.org/10.1021/acs.langmuir.1c02231.
(12) Peeples, W.; Rosen, M. K. Mechanistic Dissection of Increased Enzymatic Rate in a Phase-Separated Compartment. *Nat. Chem. Biol.* **2021**, *17* (6), 693–702. https://doi.org/10.1038/s41589-021-00801-x.
(13) Ameta, S.; Kumar, M.; Chakraborty, N.; Matsubara, Y. J.; Prashanth, S.; Gandavadi, D.; Thutupalli, S. Multispecies Autocatalytic RNA Reaction Networks in Coacervates. *Commun. Chem.* **2023**, *6* (1), 1–10. https://doi.org/10.1038/s42004-023-00887-5.
(14) Saha, B.; Chatterjee, A.; Reja, A.; Das, D. Condensates of Short Peptides and ATP for the Temporal Regulation of Cytochrome: C Activity. *Chem. Commun.* **2019**, *55* (94), 14194–14197. https://doi.org/10.1039/c9cc07358b.
(15) Crosby, J.; Treadwell, T.; Hammerton, M.; Vasilakis, K.; Crump, M. P.; Williams, D. S.; Mann, S. Stabilization and Enhanced Reactivity of Actinorhodin Polyketide Synthase Minimal Complex in Polymer–Nucleotide Coacervate Droplets. *Chem. Commun.* **2012**, *48* (97), 11832–11834. https://doi.org/10.1039/c2cc36533b.
(16) Küffner, A. M.; Prodan, M.; Zuccarini, R.; Capasso Palmiero, U.; Faltova, L.; Arosio, P. Acceleration of an Enzymatic Reaction in Liquid Phase Separated Compartments Based on Intrinsically Disordered Protein Domains. *ChemSystemsChem* **2020**, *2* (4), e2000001. https://doi.org/10.1002/syst.202000001.
(17) Nakashima, K. K.; Vibhute, M. A.; Spruijt, E. Biomolecular Chemistry in Liquid Phase Separated Compartments. *Front. Mol. Biosci.* **2019**, *6*, 21. https://doi.org/10.3389/fmolb.2019.00021.
(18) Mu, W.; Ji, Z.; Zhou, M.; Wu, J.; Lin, Y.; Qiao, Y. Membrane-Confined Liquid-Liquid Phase Separation toward Artificial Organelles. *Sci. Adv.* **2021**, *7* (22), 9000–9028. https://doi.org/10.1126/sciadv.abf9000.
(19) Lv, K.; Perriman, A. W.; Mann, S. Photocatalytic Multiphase Micro-Droplet Reactors Based on Complex Coacervation. *Chem. Commun.* **2015**, *51* (41), 8600–8602. https://doi.org/10.1039/c5cc01914a.
(20) Poudyal, R. R.; Keating, C. D.; Bevilacqua, P. C. Polyanion-Assisted Ribozyme Catalysis Inside Complex Coacervates. *ACS Chem. Biol.* **2019**, *14* (6), 1243–1248. https://doi.org/10.1021/acschembio.9b00205.
(21) Le Vay, K.; Song, E. Y.; Ghosh, B.; Tang, T. Y. D.; Mutschler, H. Enhanced Ribozyme-Catalyzed Recombination and Oligonucleotide Assembly in Peptide-RNA Condensates. *Angew. Chemie - Int. Ed.* **2021**, *60* (50), 26096–26104. https://doi.org/10.1002/anie.202109267.
(22) Le Vay, K. K.; Salibi, E.; Ghosh, B.; Dora Tang, T. Y.; Mutschler, H. Ribozyme Activity Modulates the Physical Properties of RNA–Peptide Coacervates. *Elife* **2023**, *12*. https://doi.org/10.7554/eLife.83543.
(23) Wee, W. A.; Sugiyama, H.; Park, S. Photoswitchable Single-Stranded DNA-Peptide Coacervate Formation as a Dynamic System for Reaction Control. *iScience* **2021**, *24* (12), 103455.

https://doi.org/10.1016/j.isci.2021.103455.
(24) Wang, J.; Abbas, M.; Wang, J.; Spruijt, E. Selective Amide Bond Formation in Redox-Active Coacervate Protocells. *Nat. Commun.* **2023**, *14* (1), 1–11. https://doi.org/10.1038/s41467-023-44284-x.
(25) Poudyal, R. R.; Guth-Metzler, R. M.; Veenis, A. J.; Frankel, E. A.; Keating, C. D.; Bevilacqua, P. C. Template-Directed RNA Polymerization and Enhanced Ribozyme Catalysis inside Membraneless Compartments Formed by Coacervates. *Nat. Commun.* **2019**, *10* (1), 1–13. https://doi.org/10.1038/s41467-019-08353-4.
(26) Fraccia, T. P.; Martin, N. Non-Enzymatic Oligonucleotide Ligation in Coacervate Protocells Sustains Compartment-Content Coupling. *Nat. Commun.* **2023**, *14* (1), 1–12. https://doi.org/10.1038/s41467-023-38163-8.
(27) Sokolova, E.; Spruijt, E.; Hansen, M. M. K.; Dubuc, E.; Groen, J.; Chokkalingam, V.; Piruska, A.; Heus, H. A.; Huck, W. T. S. Enhanced Transcription Rates in Membrane-Free Protocells Formed by Coacervation of Cell Lysate. *Proc. Natl. Acad. Sci. U. S. A.* **2013**, *110* (29), 11692–11697. https://doi.org/10.1073/pnas.1222321110.
(28) Weber, C.; Michaels, T.; Mahadevan, L. Spatial Control of Irreversible Protein Aggregation. *Elife* **2019**, *8*. https://doi.org/10.7554/eLife.42315.
(29) Michaels, T. C. T.; Mahadevan, L.; Weber, C. A. Enhanced Potency of Aggregation Inhibitors Mediated by Liquid Condensates. *Phys. Rev. Res.* **2022**, *4* (4), 043173. https://doi.org/10.1103/PhysRevResearch.4.043173.
(30) Laha, S.; Bauermann, J.; Jülicher, F.; Michaels, T. C. T.; Weber, C. A. Chemical Reactions Regulated by Phase-Separated Condensates. *arXiv* **2024**, *2403.05228*. https://doi.org/10.48550/arXiv.2403.05228.
(31) Fan, W. Percolation Theory Used to Design Biomolecular Condensates. *bioRxiv* **2023**, 2023.11.04.565634. https://doi.org/10.1101/2023.11.04.565634.
(32) Bauermann, J.; Laha, S.; McCall, P. M.; Jülicher, F.; Weber, C. A. Chemical Kinetics and Mass Action in Coexisting Phases. *J. Am. Chem. Soc.* **2022**, *144* (42), 19294–19304. https://doi.org/10.1021/jacs.2c06265.
(33) Mattiello, S.; Ghiglietti, E.; Zucchi, A.; Beverina, L. Selectivity in Micellar Catalysed Reactions: The Role of Interfacial Dipole, Compartmentalisation, and Specific Interactions with the Surfactants. *Curr. Opin. Colloid Interface Sci.* **2023**, *64*, 101681. https://doi.org/10.1016/j.cocis.2023.101681.
(34) Dumelie, J. G.; Chen, Q.; Miller, D.; Attarwala, N.; Gross, S. S.; Jaffrey, S. R. Biomolecular Condensates Create Phospholipid-Enriched Microenvironments. *Nat. Chem. Biol.* **2023**, 1–12. https://doi.org/10.1038/s41589-023-01474-4.
(35) Thody, S. A.; Clements, H. D.; Baniasadi, H.; Lyon, A. S.; Sigman, M. S.; Rosen, M. K. Small Molecule Properties Define Partitioning into Biomolecular Condensates. *bioRxiv* **2022**, 2022.12.19.521099. https://doi.org/10.1101/2022.12.19.521099.
(36) Frankel, E. A.; Bevilacqua, P. C.; Keating, C. D. Polyamine/Nucleotide Coacervates Provide Strong Compartmentalization of Mg2+, Nucleotides, and RNA. *Langmuir* **2016**, *32* (8), 2041–2049. https://doi.org/10.1021/acs.langmuir.5b04462.
(37) Wang, Q.; Schlenoff, J. B. The Polyelectrolyte Complex/Coacervate Continuum. *Macromolecules* **2014**, *47* (9), 3108–3116. https://doi.org/10.1021/ma500500q.
(38) Gody, G.; Zetterlund, P. B.; Perrier, S.; Harrisson, S. The Limits of Precision Monomer Placement in Chain Growth Polymerization. *Nat. Commun.* **2016**, *7* (1), 1–8. https://doi.org/10.1038/ncomms10514.
(39) Zhou, Y. N.; Li, J. J.; Wang, T. T.; Wu, Y. Y.; Luo, Z. H. Precision Polymer Synthesis by Controlled Radical Polymerization: Fusing the Progress from Polymer Chemistry and Reaction Engineering. *Prog. Polym. Sci.* **2022**, *130*, 101555. https://doi.org/10.1016/j.progpolymsci.2022.101555.
(40) Kang, J.; Miyajima, D.; Mori, T.; Inoue, Y.; Itoh, Y.; Aida, T. A Rational Strategy for the

Realization of Chain-Growth Supramolecular Polymerization. *Science* **2015**, *347* (6222), 646–651. https://doi.org/10.1126/science.aaa4249.
(41) Canavelli, P.; Islam, S.; Powner, M. W. Peptide Ligation by Chemoselective Aminonitrile Coupling in Water. *Nature* **2019**, *571* (7766), 546–549. https://doi.org/10.1038/s41586-019-1371-4.
(42) Müller, F.; Escobar, L.; Xu, F.; Węgrzyn, E.; Nainytė, M.; Amatov, T.; Chan, C. Y.; Pichler, A.; Carell, T. A Prebiotically Plausible Scenario of an RNA–Peptide World. *Nature* **2022**, *605* (7909), 279–284. https://doi.org/10.1038/s41586-022-04676-3.
(43) Liu, R.; Orgel, L. E. Polymerization on the Rocks: β-Amino Acids and Arginine. *Orig. Life Evol. Biosph.* **1998**, *28* (3), 245–257. https://doi.org/10.1023/A:1006576213220.
(44) Frenkel-Pinter, M.; Haynes, J. W.; Mohyeldin, A. M.; Martin, C.; Sargon, A. B.; Petrov, A. S.; Krishnamurthy, R.; Hud, N. V.; Williams, L. D.; Leman, L. J. Mutually Stabilizing Interactions between Proto-Peptides and RNA. *Nat. Commun.* **2020**, *11* (1), 1–14. https://doi.org/10.1038/s41467-020-16891-5.
(45) Frenkel-Pinter, M.; Bouza, M.; Fernández, F. M.; Leman, L. J.; Williams, L. D.; Hud, N. V.; Guzman-Martinez, A. Thioesters Provide a Plausible Prebiotic Path to Proto-Peptides. *Nat. Commun.* **2022**, *13* (1), 1–8. https://doi.org/10.1038/s41467-022-30191-0.
(46) Frenkel-Pinter, M.; Haynes, J. W.; Martin, C.; Petrov, A. S.; Burcar, B. T.; Krishnamurthy, R.; Hud, N. V.; Leman, L. J.; Williams, L. D. Selective Incorporation of Proteinaceous over Nonproteinaceous Cationic Amino Acids in Model Prebiotic Oligomerization Reactions. *Proc. Natl. Acad. Sci. U. S. A.* **2019**, *116* (33), 16338–16346. https://doi.org/10.1073/pnas.1904849116.
(47) Kamagata, K.; Iwaki, N.; Kanbayashi, S.; Banerjee, T.; Chiba, R.; Gaudon, V.; Castaing, B.; Sakomoto, S. Structure-Dependent Recruitment and Diffusion of Guest Proteins in Liquid Droplets of FUS. *Sci. Rep.* **2022**, *12* (1), 1–11. https://doi.org/10.1038/s41598-022-11177-w.
(48) Coupe, S.; Fakhri, N. ATP-Induced Cross-Linking of a Biomolecular Condensate. *Biophys. J.* **2023**. https://doi.org/10.1016/j.bpj.2023.07.013.
(49) Duim, H.; Otto, S. Towards Open-Ended Evolution in Self-Replicating Molecular Systems. *Beilstein J. Org. Chem.* **2017**, *13*, 1189–1203. https://doi.org/10.3762/bjoc.13.118.
(50) Le Vay, K.; Weise, L. I.; Libicher, K.; Mascarenhas, J.; Mutschler, H. Templated Self-Replication in Biomimetic Systems. *Adv. Biosyst.* **2019**, *3* (6), 1800313. https://doi.org/10.1002/adbi.201800313.
(51) Zielinski, W. S.; Orgel, L. E. Autocatalytic Synthesis of a Tetranucleotide Analogue. *Nature* **1987**, *327* (6120), 346–347. https://doi.org/10.1038/327346a0.
(52) von Kiedrowski, G. A Self-Replicating Hexadeoxynucleotide. *Angew. Chemie Int. Ed. English* **1986**, *25* (10), 932–935. https://doi.org/10.1002/anie.198609322.
(53) Lee, D. H.; Granja, J. R.; Martinez, J. A.; Severin, K.; Ghadiri, M. R. A Self-Replicating Peptide. *Nature* **1996**, *382* (6591), 525–528. https://doi.org/10.1038/382525a0.
(54) Rubinov, B.; Wagner, N.; Rapaport, H.; Ashkenasy, G. Self-Replicating Amphiphilic β-Sheet Peptides. *Angew. Chemie - Int. Ed.* **2009**, *48* (36), 6683–6686. https://doi.org/10.1002/anie.200902790.
(55) Paul, N.; Joyce, G. F. A Self-Replicating Ligase Ribozyme. *Proc. Natl. Acad. Sci. U. S. A.* **2002**, *99* (20), 12733–12740. https://doi.org/10.1073/pnas.202471099.
(56) Lincoln, T. A.; Joyce, G. F. Self-Sustained Replication of an RNA Enzyme. *Science* **2009**, *323* (5918), 1229–1232. https://doi.org/10.1126/science.1167856.
(57) Vaidya, N.; Manapat, M. L.; Chen, I. A.; Xulvi-Brunet, R.; Hayden, E. J.; Lehman, N. Spontaneous Network Formation among Cooperative RNA Replicators. *Nature* **2012**, *491* (7422), 72–77. https://doi.org/10.1038/nature11549.
(58) Carnall, J. M. A.; Waudby, C. A.; Belenguer, A. M.; Stuart, M. C. A.; Peyralans, J. J. P.; Otto, S. Mechanosensitive Self-Replication Driven by Self-Organization. *Science* **2010**, *327* (5972), 1502–1506. https://doi.org/10.1126/science.1182767.

(59) Tjivikua, T.; Ballester, P.; Rebek, J. A Self-Replicating System. *J. Am. Chem. Soc.* **1990**, *112* (3), 1249–1250. https://doi.org/10.1021/ja00159a057.
(60) Nott, T. J.; Craggs, T. D.; Baldwin, A. J. Membraneless Organelles Can Melt Nucleic Acid Duplexes and Act as Biomolecular Filters. *Nat. Chem.* **2016**, *8* (6), 569–575. https://doi.org/10.1038/nchem.2519.
(61) Cakmak, F. P.; Choi, S.; Meyer, M. C. O.; Bevilacqua, P. C.; Keating, C. D. Prebiotically-Relevant Low Polyion Multivalency Can Improve Functionality of Membraneless Compartments. *Nat. Commun.* **2020**, *11* (1). https://doi.org/10.1038/s41467-020-19775-w.
(62) Iglesias-Artola, J. M.; Drobot, B.; Kar, M.; Fritsch, A. W.; Mutschler, H.; Dora Tang, T. Y.; Kreysing, M. Charge-Density Reduction Promotes Ribozyme Activity in RNA–Peptide Coacervates via RNA Fluidization and Magnesium Partitioning. *Nat. Chem.* **2022**, *14* (4), 407–416. https://doi.org/10.1038/s41557-022-00890-8.
(63) Issac, R.; Chmielewski, J. Approaching Exponential Growth with a Self-Replicating Peptide. *J. Am. Chem. Soc.* **2002**, *124* (24), 6808–6809. https://doi.org/10.1021/ja026024i.
(64) Cakmak, F. P.; Choi, S.; Meyer, M. C. O.; Bevilacqua, P. C.; Keating, C. D. Prebiotically-Relevant Low Polyion Multivalency Can Improve Functionality of Membraneless Compartments. *Nat. Commun.* **2020**, *11* (1). https://doi.org/10.1038/s41467-020-19775-w.
(65) Dunlap, J. C. Molecular Bases for Circadian Clocks. *Cell* **1999**, *96* (2), 271–290. https://doi.org/10.1016/S0092-8674(00)80566-8.
(66) Goldbeter, A.; Berridge, M. J. *Biochemical Oscillations and Cellular Rhythms*; Cambridge University Press, 1996. https://doi.org/10.1017/cbo9780511608193.
(67) Novák, B.; Tyson, J. J. Design Principles of Biochemical Oscillators. *Nat. Rev. Mol. Cell Biol.* **2008**, *9* (12), 981–991. https://doi.org/10.1038/nrm2530.
(68) Semenov, S. N.; Wong, A. S. Y.; Van Der Made, R. M.; Postma, S. G. J.; Groen, J.; Van Roekel, H. W. H.; De Greef, T. F. A.; Huck, W. T. S. Rational Design of Functional and Tunable Oscillating Enzymatic Networks. *Nat. Chem. 2014 72* **2015**, *7* (2), 160–165. https://doi.org/10.1038/nchem.2142.
(69) Prigogine, I.; Lefever, R. Symmetry Breaking Instabilities in Dissipative Systems. II. *J. Chem. Phys.* **1968**, *48* (4), 1695–1700. https://doi.org/10.1063/1.1668896.
(70) Yoshida, R. Self-Oscillating Gels Driven by the Belousov-Zhabotinsky Reaction as Novel Smart Materials. *Adv. Mater.* **2010**, *22* (31), 3463–3483. https://doi.org/10.1002/adma.200904075.
(71) Vanag, V. K.; Epstein, I. R. Pattern Formation in a Tunable Medium: The Belousov-Zhabotinsky Reaction in an Aerosol OT Microemulsion. *Phys. Rev. Lett.* **2001**, *87* (22), 228301-228301–228304. https://doi.org/10.1103/PhysRevLett.87.228301.
(72) ter Harmsel, M.; Maguire, O. R.; Runikhina, S. A.; Wong, A. S. Y.; Huck, W. T. S.; Harutyunyan, S. R. A Catalytically Active Oscillator Made from Small Organic Molecules. *Nature* **2023**, *621* (7977), 87–93. https://doi.org/10.1038/s41586-023-06310-2.
(73) Zhang, Y.; Pyo, A. G. T.; Jiang, Y.; Brangwynne, C. P.; Stone, H. A.; Wingreen, N. S.; Pyo, A. G. T.; Brangwynne, C. P.; Stone, H. A.; Wingreen, N. S.; Zhang, Y. Interface Resistance of Biomolecular Condensates. *Elife* **2023**, *12*, RP91680. https://doi.org/10.7554/eLife.91680.1.

Table of content graphic

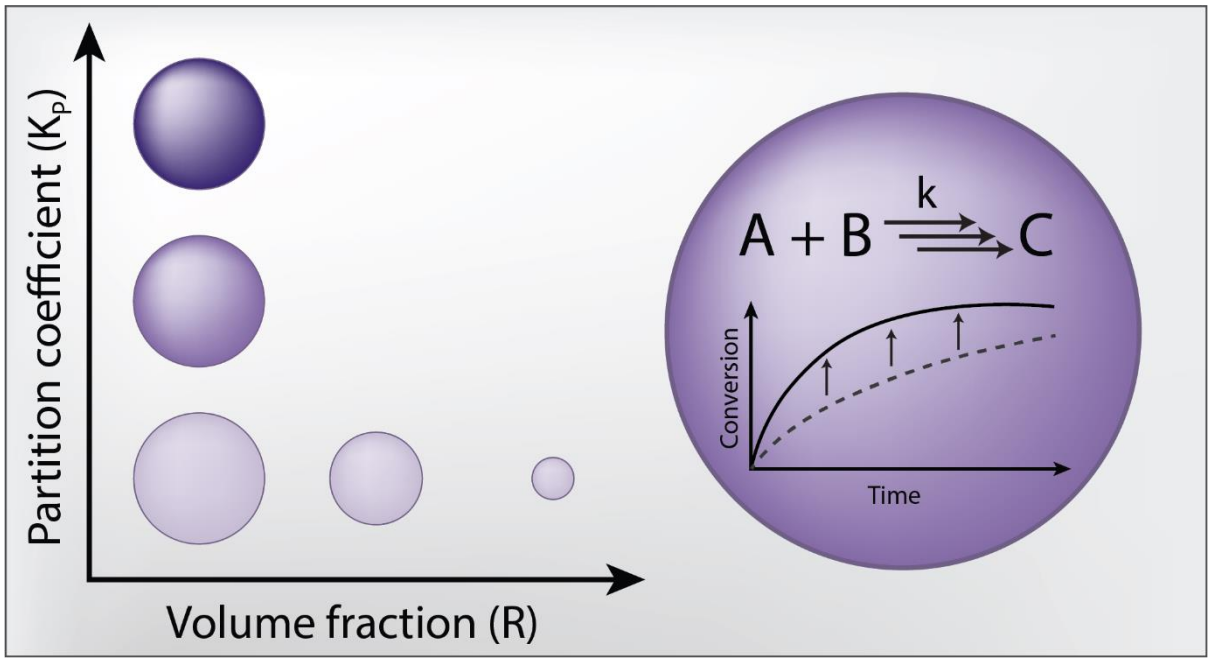

Supplementary Information

Phase-separated droplets can direct the kinetics of chemical reactions including polymerization, self-replication and oscillating networks

Iris B. A. Smokers[‡][a], Brent S. Visser[‡][a], Wojciech P. Lipiński[a], Karina K. Nakashima[a],[b] and Evan Spruijt*[a]

[a] Institute for Molecules and Materials, Radboud University, Heyendaalseweg 135, 6523 AJ Nijmegen, The Netherlands

[b] Current address: Institut de Science et d'Ingénierie Supramoléculaires (ISIS), CNRS UMR 7006, Université de Strasbourg, 8 Allée Gaspard Monge, Strasbourg 67000, France

‡ These authors contributed equally. * Corresponding author, e-mail: e.spruijt@science.ru.nl

Contents

1. Rate equations and model parameters

1.1. Bimolecular reaction

For the simulations of the bimolecular reaction, we used the following reaction steps:

$$A + B \overset{k}{\rightarrow} C$$

Which could take place in both phases with the following transfer between the phases:

$$\frac{d[A_{\mathrm{dil}}]}{dt} = -K_P * k_T * [A_{\mathrm{dil}}] + k_T * [A_{\mathrm{coac}}]$$

$$\frac{d[A_{\mathrm{coac}}]}{dt} = K_P * k_T * [A_{\mathrm{dil}}] * R - k_T * [A_{\mathrm{coac}}] * R$$

Where the subscript *coac* denotes a species in the dense phase, the subscript *dil* denotes a species in the dilute phase, and *kt* is the rate of transfer between phases, chosen to be sufficiently large to mimic near instantaneous transport. *R* denotes the volume ratio dilute/dense.

This results in the following rate equations:

Supplementary Table 1: Reaction steps and rate equations for the bimolecular reaction in a two-phase system.

Reaction	ODE
$\boldsymbol{A_{\mathrm{dil}} + B_{\mathrm{dil}} \overset{k}{\rightarrow} C_{\mathrm{dil}}}$	$\frac{d[A]}{dt} = -k[A_{\mathrm{dil}}] * [B_{\mathrm{dil}}]$ $\frac{d[B]}{dt} = -k[AA_{\mathrm{dil}}] * [B_{\mathrm{dil}}]$ $\frac{d[C]}{dt} = k[AA_{\mathrm{dil}}] * [B_{\mathrm{dil}}]$
$\boldsymbol{A_{\mathrm{coac}} + B_{\mathrm{coac}} \overset{k}{\rightarrow} C_{\mathrm{coac}}}$	$\frac{d[A_{\mathrm{in}}]}{dt} = -k[A_{\mathrm{coac}}] * [B_{\mathrm{coac}}]$ $\frac{d[B_{\mathrm{in}}]}{dt} = -k[A_{\mathrm{coac}}] * [B_{\mathrm{coac}}]$ $\frac{d[C_{\mathrm{in}}]}{dt} = k[A_{\mathrm{coac}}] * [B_{\mathrm{coac}}]$

Transport of all species X $\boldsymbol{X_{dil} \xrightarrow{k_T} X_{coac}}$ $\boldsymbol{X_{coac} \xrightarrow{k_T} X_{dil}}$	$\frac{d[X_{dil}]}{dt} = -K_P * k_T * [X_{dil}] + k_T * [X_{coac}]$ $\frac{d[X_{dil}]}{dt} = K_P * k_T * [X_{dil}] * R - k_T * [X_{coac}] * R$

We used the following input parameters for the rate constant and total starting concentration of all species:

$k = 0.1\ \mu M^{-1}\ min^{-1}$

$[A_{tot}] = 1\ \mu M$

$[B_{tot}] = 1\ \mu M$

$[C_{tot}] = 0\ \mu M$

$k_T = 10\ min^{-1}$

Starting concentrations of dilute and dense phase concentrations of all species were initialized at equilibrium according to R and K_P, determined by the following equations:

$$X_{dil} = \frac{1+R}{K_P+R}[X_{tot}]$$

$$X_{coac} = K_P * \frac{1+R}{K_P+R}[X_{tot}]$$

1.2. Polymerization reaction

To simulate the polymerization reaction, an array representing the monomer concentration and polymer lengths up to n=200 was initialized. The following reactions were simulated:

Supplementary Table 2: Reaction steps and rate equations for the polymerization reaction in a two-phase system.

Reaction	ODE
$\boldsymbol{M_{dil} + M_{dil} \xrightarrow{k_{init}} P_{2\ dil}}$	$\frac{d[M_{dil}]}{dt} = -2k_{init}[M_{dil}]^2$ $\frac{d[P_{2\ dil}]}{dt} = 2k_{init}[M_{dil}]^2$

$\boldsymbol{P_{n\,\mathrm{dil}} + M_{\mathrm{dil}} \xrightarrow{k_{\mathrm{prop}}} P_{n+1\,\mathrm{dil}}}$	$\frac{d[P_{n\,\mathrm{dil}}]}{dt} = k_{\mathrm{prop}} * [P_{n-1\,\mathrm{dil}}] * [M_{\mathrm{dil}}]$ $\frac{d[P_{n\,\mathrm{dil}}]}{dt} = -k_{\mathrm{prop}} * [P_{n\,\mathrm{dil}}] * [M_{\mathrm{dil}}]$ $\frac{d[M_{\mathrm{dil}}]}{dt} = -k_{\mathrm{prop}} * [P_{n-1\,\mathrm{dil}}] * [M_{\mathrm{dil}}]$
$\boldsymbol{M_{\mathrm{coac}} + M_{\mathrm{coac}} \xrightarrow{k_{\mathrm{init}}} P_{2\,\mathrm{coac}}}$	$\frac{d[M_{\mathrm{coac}}]}{dt} = -2k_{\mathrm{init}}[M_{\mathrm{coac}}]^2$ $\frac{d[P_{2\,\mathrm{coac}}]}{dt} = 2k_{\mathrm{init}}[M_{\mathrm{coac}}]^2$
$\boldsymbol{P_{n\,\mathrm{coac}} + M_{\mathrm{coac}} \xrightarrow{k_{\mathrm{prop}}} P_{n+1\,\mathrm{coac}}}$	$\frac{d[P_{n\,\mathrm{coac}}]}{dt} = k_{\mathrm{prop}} * [P_{n-1\,\mathrm{coac}}] * [M_{\mathrm{coac}}]$ $\frac{d[P_{n\,\mathrm{coac}}]}{dt} = -k_{\mathrm{prop}} * [P_{n\,\mathrm{coac}}] * [M_{\mathrm{coac}}]$ $\frac{d[M_{\mathrm{coac}}]}{dt} = -k_{\mathrm{prop}} * [P_{n-1\,\mathrm{coac}}] * [M_{\mathrm{coac}}]$
Transport of monomer $\boldsymbol{M_{\mathrm{dil}} \xrightarrow{k_T} M_{\mathrm{coac}}}$ $\boldsymbol{M_{\mathrm{coac}} \xrightarrow{k_T} M_{\mathrm{dil}}}$	$\frac{d[M_{\mathrm{dil}}]}{dt} = -K_P * k_T * [M_{\mathrm{dil}}] + k_T * [M_{\mathrm{coac}}]$ $\frac{d[M_{\mathrm{coac}}]}{dt} = K_P * k_T * [M_{\mathrm{dil}}] * R - k_T * [M_{\mathrm{coac}}] * R$
Transport of polymer $\boldsymbol{P_{n\,\mathrm{dil}} \xrightarrow{k_T} P_{n\,\mathrm{coac}}}$ $\boldsymbol{P_{n\,\mathrm{coac}} \xrightarrow{k_T} P_{n\,\mathrm{dil}}}$	$\frac{d[P_{n\,\mathrm{dil}}]}{dt} = -K_P * k_T * [P_{n\,\mathrm{dil}}] +$ $e^{-n*\gamma} * k_T * [P_{n\,\mathrm{coac}}]$ $\frac{d[P_{n\,\mathrm{coac}}]}{dt} = K_P * k_T * [P_{n\,\mathrm{dil}}] * R -$ $e^{-n*\gamma} * k_T * [P_{n\,\mathrm{coac}}] * R$

We used the following input parameters:

$k_{\mathrm{init}} = 0.1\ \mu\mathrm{M}^{-1}\ \mathrm{min}^{-1}$

$k_{\mathrm{prop}} = 5 * 10^{-5}\ \mu\mathrm{M}^{-1}\ \mathrm{min}^{-1}$

$[M_{\mathrm{tot}}] = 100\ \mu\mathrm{M}$

$k_T = 10\ \mathrm{min}^{-1}$

$\gamma = 1/25$

Starting concentrations per phase were initialized as in the bimolecular reaction.

1.3 Self-replicator

This results in the following rate equations were used to simulate the self-replicator, where the subscript *phase* denotes either the coacervate or dilute phase:

Supplementary Table 3: Reaction steps and rate equations for the self-replication reaction in a two-phase system.

Reaction	ODE
$\boldsymbol{A}_{\mathbf{phase}} + \boldsymbol{B}_{\mathbf{phase}} \xrightarrow{k_{\mathbf{bimol}}} \boldsymbol{T}_{\mathbf{phase}}$	$\frac{d[A_{\mathrm{phase}}]}{dt} = -k_{\mathrm{bimol}}[A_{\mathrm{phase}}][B_{\mathrm{phase}}]$ $\frac{d[B_{\mathrm{phase}}]}{dt} = -k_{\mathrm{bimol}}[A_{\mathrm{phase}}][B_{\mathrm{phase}}]$ $\frac{d[T_{\mathrm{phase}}]}{dt} = k_{\mathrm{bimol}}[A_{\mathrm{phase}}][B_{\mathrm{phase}}]$
$\boldsymbol{A}_{\mathbf{phase}} + \boldsymbol{B}_{\mathbf{phase}} + \boldsymbol{T}_{\mathbf{phase}} \xrightarrow{k_{\mathbf{templ}}} \boldsymbol{ABT}_{\mathbf{phase}}$	$\frac{d[A_{\mathrm{phase}}]}{dt} = -k_{\mathrm{templ}}[A_{\mathrm{phase}}][B_{\mathrm{phase}}][T_{\mathrm{phase}}]$ $\frac{d[B_{\mathrm{phase}}]}{dt} = -k_{\mathrm{templ}}[A_{\mathrm{phase}}][B_{\mathrm{phase}}][T_{\mathrm{phase}}]$ $\frac{d[T_{\mathrm{phase}}]}{dt} = -k_{\mathrm{templ}}[A_{\mathrm{phase}}][B_{\mathrm{phase}}][T_{\mathrm{phase}}]$ $\frac{d[ABT_{\mathrm{phase}}]}{dt} = k_{\mathrm{templ}}[A_{\mathrm{phase}}][B_{\mathrm{phase}}][T_{\mathrm{phase}}]$

$\boldsymbol{ABT_{phase} \xrightarrow{k_{templ\ rev}} A_{phase} + B_{phase} + T_{phase}}$	$\frac{d[A_{phase}]}{dt} = k_{templ\ rev}[ABT_{phase}]$ $\frac{d[B_{phase}]}{dt} = k_{templ\ rev}[ABT_{phase}]$ $\frac{d[T_{phase}]}{dt} = k_{templ\ rev}[ABT_{phase}]$ $\frac{d[ABT_{phase}]}{dt} = -k_{templ\ rev}[ABT_{phase}]$
$\boldsymbol{ABT_{phase} \xrightarrow{k_{lig}} TT_{phase}}$	$\frac{d[ABT_{phase}]}{dt} = -k_{lig}[ABT_{phase}]$ $\frac{d[TT_{phase}]}{dt} = k_{lig}[ABT_{phase}]$
$\boldsymbol{TT_{phase} \xrightarrow{k_{lig\ rev}} ABT_{phase}}$	$\frac{d[ABT_{phase}]}{dt} = k_{lig\ rev}[TT_{phase}]$ $\frac{d[TT_{phase}]}{dt} = -k_{lig\ rev}[TT_{phase}]$
$\boldsymbol{TT_{phase} \xrightarrow{k_{dis}} 2T_{phase}}$	$\frac{d[TT_{phase}]}{dt} = -k_{dis}[TT_{phase}]$ $\frac{d[T_{phase}]}{dt} = -2k_{dis}[TT_{phase}]$
$\boldsymbol{2T_{phase} \xrightarrow{k_{dis\ rev}} TT_{phase}}$	$\frac{d[T_{phase}]}{dt} = -2k_{dis\ rev}[T_{phase}]^2$ $\frac{d[TT_{phase}]}{dt} = k_{dis\ rev}[T_{phase}]^2$
Transport of all species X $\boldsymbol{X_{dil} \xrightarrow{k_T} X_{coac}}$ $\boldsymbol{X_{coac} \xrightarrow{k_T} X_{dil}}$	$\frac{d[X_{dil}]}{dt} = -K_P * k_T * [X_{dil}] + k_T * [X_{coac}]$ $\frac{d[X_{dil}]}{dt} = K_P * k_T * [X_{dil}] * R - k_T * [X_{coac}] * R$

We used the following input parameters:

$k_{\text{bimol}} = 0.073\ \mu\text{M}^{-1}\ \text{min}^{-1}$
$k_{\text{templ}} = 0.4\ \mu\text{M}^{-2}\ \text{min}^{-1}$
$k_{\text{templ rev}} = 0.3\ \text{min}^{-1}$
$k_{\text{lig}} = 1.2\ \text{min}^{-1}$
$k_{\text{dis}} = 0.3\ \text{min}^{-1}$
$k_{\text{dis rev}} = 0.3\ \mu\text{M}^{-1}\ \text{min}^{-1}$
$k_T = 10\ \text{min}^{-1}$

$[A_{\text{tot}}] = 1\ \mu\text{M}$
$[B_{\text{tot}}] = 1\ \mu\text{M}$
$[T_{\text{tot}}] = 0\ \mu\text{M}$
$[ABT_{\text{tot}}] = 0\ \mu\text{M}$
$[TT_{\text{tot}}] = 0\ \mu\text{M}$

Starting concentrations per phase were initialized as in the bimolecular reaction.

1.4 Oscillator

For the Brusselator, [A], [B], [C], and [D] are constant and not included in the ODEs. The subscript *phase* denotes either the coacervate or dilute phase.

Supplementary Table 4: Reaction steps and rate equations for the Brusselator oscillating reaction network in a two-phase system.

Reaction	ODE
$\boldsymbol{A_{\text{phase}} \xrightarrow{k_1} X_{\text{phase}}}$	$\frac{d[X_{\text{phase}}]}{dt} = k_1[A_{\text{phase}}]$
$\boldsymbol{X_{\text{phase}} + B_{\text{phase}} \xrightarrow{k_2} Y_{\text{phase}} + C_{\text{phase}}}$	$\frac{d[X_{\text{phase}}]}{dt} = -k_2[B_{\text{phase}}][X_{\text{phase}}]$ $\frac{d[Y_{\text{phase}}]}{dt} = k_2[B_{\text{phase}}][X_{\text{phase}}]$

$\mathbf{2X_{phase} + Y_{phase} \overset{k_3}{\rightarrow} 3X_{phase}}$	$\frac{d[X_{\text{phase}}]}{dt} = k_3[X_{\text{phase}}]^2[Y_{\text{phase}}]$ $\frac{d[Y_{\text{phase}}]}{dt} = -k_3[X_{\text{phase}}]^2[Y_{\text{phase}}]$
$\mathbf{X_{phase} \overset{k_4}{\rightarrow} D_{phase}}$	$\frac{d[X_{\text{phase}}]}{dt} = -k_4[X_{\text{phase}}]$
Transport of all species N $\mathbf{N_{dil} \overset{k_T}{\rightarrow} N_{coac}}$ $\mathbf{N_{coac} \overset{k_T}{\rightarrow} N_{dil}}$	$\frac{d[N_{\text{dil}}]}{dt} = -K_P * k_T * [N_{\text{dil}}] + k_T * [N_{\text{coac}}]$ $\frac{d[N_{\text{dil}}]}{dt} = K_P * k_T * [N_{\text{dil}}] * R - k_T * [N_{\text{coac}}] * R$

We used the following input parameters:

$k_1 = 0.5\ \text{s}^{-1}$

$k_2 = 0.5\ \mu\text{M}^{-1}\ \text{s}^{-1}$

$k_3 = 0.5\ \mu\text{M}^{-2}\ \text{s}^{-1}$

$k_4 = 0.1\ \text{s}^{-1}$

$k_T = 10\ \text{min}^{-1}$

$[A_{\text{tot}}] = 0.05\ \mu\text{M}$

$[B_{\text{tot}}] = 0.5\ \mu\text{M}$

Starting concentrations per phase, including the constant [A] and [B], were initialized as in the bimolecular reaction.

2. Supplementary results for the bimolecular reaction

2.1. Analytical derivation of relation between R and K_P for maximum rate enhancement

1st order $A \rightarrow C$

$$[A]_{\text{coac}} = \frac{K_P(1+R)}{R+K_P}[A]_{\text{tot}}$$

$$[A]_{\text{dil}} = \frac{1+R}{R+K_P}[A]_{\text{tot}}$$

Reaction rate in a phase-separated system (r_s) and homogenous system (r_h):

$$r_s = k\frac{1}{1+R}[A]_{\text{coac}} + k\frac{R}{1+R}[A]_{\text{dil}}$$

$$r_s = k\frac{1}{1+R}\cdot\frac{K_P(1+R)}{R+K_P}[A]_{\text{tot}} + k\frac{\text{R}}{1+R}\cdot\frac{1+R}{R+K_P}[A]_{\text{tot}} = k[A]_{\text{tot}}$$

$$r_h = k[A]_{\text{tot}}$$

$$r_h = r_s$$

2nd order $A + A \rightarrow C$

Relation between total concentration and concentration in each phase (assuming infinitely fast transport):

$$[A]_{\text{coac}} = \frac{K_P(1+R)}{R+K_P}[A]_{\text{tot}}$$

$$[A]_{\text{dil}} = \frac{1+R}{R+K_P}[A]_{\text{tot}}$$

Reaction rate in a phase-separated system (r_s) and homogenous system (r_h):

$$r_s = k\frac{1}{1+R}[A]_{\text{coac}}{}^2 + k\frac{R}{1+R}[A]_{\text{dil}}{}^2$$

$$r_s = k\frac{1}{1+R}\left(\frac{K_P(1+R)}{K_P+R}\right)^2[A]_{\text{tot}}{}^2 + k\frac{R}{1+R}\left(\frac{1+R}{R+K_P}\right)^2[A]_{\text{tot}}{}^2$$

$$r_h = k[A]_{\text{tot}}{}^2$$

Apparent reaction rate constant in a phase-separated system (k^*) and ratio of the apparent phase-separated and homogenous rate constants:

$$k^* = k\left(\frac{1}{1+R}\cdot\left(\frac{K_P(1+R)^2}{K_P+R}\right)^2 + \left(\frac{1+R}{R+K_P}\right)^2\cdot\frac{R}{1+R}\right)$$

$$\frac{k^*}{k} = \frac{{K_P}^2(1+R)}{(K_P+R)^2} + \frac{R(1+R)}{(K_P+R)^2} = \frac{({K_P}^2+R)(1+R)}{(K_P+R)^2}$$

Finding R which gives the maximal rate enhancement:

$$\frac{d}{dR}\left(\frac{k^*}{k}\right) = \frac{d}{dR}\left(\frac{({K_P}^2+R)(1+R)}{(K_P+R)^2}\right) = \frac{(-1+K_P)^2(K_P-R)}{(K_P+R)^3}$$

$$\frac{d}{dR}\left(\frac{k^*}{k}\right) = 0 \;\Leftrightarrow\; K_P - R = 0; R = K_P$$

<u>2nd order $A + B \rightarrow C$</u>

Relation between total concentration and concentration in each phase (assuming infinitely fast transport, same relation applies for B as well):

$$[A]_{\text{coac}} = \frac{K_{P,A}(1+R)}{R+K_{P,A}}[A]_{\text{tot}}$$

$$[A]_{\text{dil}} = \frac{1+R}{R+K_{P,A}}[A]_{\text{tot}}$$

Reaction rate in a phase-separated system (r_s) and homogenous system (r_h):

$$r_s = k\frac{1}{1+R}[A]_{\text{coac}}[B]_{\text{coac}} + \mathrm{k}\frac{R}{1+R}[A]_{\text{dil}}[B]_{\text{dil}}$$

$$r_s = k\frac{1}{1+R}\cdot\frac{K_{P,A}(1+R)}{K_{P,A}+R}\cdot\frac{K_{P,B}(1+R)}{K_{P,B}+R}[A]_{\text{tot}}[B]_{\text{tot}} + \mathrm{k}\frac{R}{1+R}\cdot\frac{1+R}{K_{P,A}+R}\cdot\frac{1+R}{K_{P,B}+R}[A]_{\text{tot}}[B]_{\text{tot}}$$

$$r_h = k[A]_{\text{tot}}[B]_{\text{tot}}$$

Ratio of the apparent phase-separated and homogenous rate constants:

$$\frac{k^*}{k} = \frac{1}{1+R}\cdot\frac{K_{P,A}(1+R)}{K_{P,A}+R}\cdot\frac{K_{P,B}(1+R)}{K_{P,B}+R} + \frac{R}{1+R}\cdot\frac{1+R}{K_{P,A}+R}\cdot\frac{1+R}{K_{P,B}+R}$$

$$= \frac{K_{P,A}K_{P,B}(1+R)}{(K_{P,A}+R)(K_{P,B}+R)} + \frac{R(1+R)}{(K_{P,A}+R)(K_{P,B}+R)} = \frac{K_{P,A}K_{P,B}(1+R)+R(1+R)}{(K_{P,A}+R)(K_{P,B}+R)}$$

Finding R which gives the maximal rate enhancement:

$$\frac{d}{dR}\left(\frac{k^*}{k}\right) = \frac{d}{dR}\left(\frac{K_{P,A}K_{P,B}(1+R)+R(1+R)}{(K_{P,A}+R)(K_{P,B}+R)}\right) = \frac{(-1+K_{P,A})(-1+K_{P,B})(K_{P,A}K_{P,B}-R^2)}{(K_{P,A}+R)^2(K_{P,B}+R)^2}$$

$$\frac{d}{dR}\left(\frac{k^*}{k}\right) = 0 \;\Leftrightarrow\; K_{P,A}K_{P,B} - R^2 = 0; K_{P,A}K_{P,B} = R^2$$

2nd order $A + A \rightarrow C$, with altered reaction rate constant in the coacervate phase

Reaction rate in a phase-separated system (r_s) and homogenous system (r_h):

$$\alpha = \frac{k_{\text{coac}}}{k_{\text{dil}}}$$

$$r_s = k_{\text{coac}}\frac{1}{1+R}[A]_{\text{coac}}{}^2 + k_{\text{dil}}\frac{R}{1+R}[A]_{\text{dil}}{}^2$$

$$r_s = \alpha k_{\text{dil}}\frac{1}{1+R}\cdot\left(\frac{K_P(1+R)}{K_P+R}\right)^2[A]_{\text{tot}}{}^2 + k_{\text{dil}}\frac{\mathrm{R}}{1+R}\left(\frac{1+R}{R+K_P}\right)^2[A]_{\text{tot}}{}^2$$
$$= k_{\text{dil}}[A]_{\text{tot}}{}^2\frac{1}{1+R}\left(R+\alpha K_P{}^2\right)$$

Assuming that the rate constant in the dilute phase is the same as in the homogeneous system:

$$r_h = k_{\text{dil}}[A]_{\text{tot}}{}^2$$

Ratio of the apparent phase-separated and homogenous rate constants:

$$\frac{k^*}{k_{\text{dil}}} = \frac{(1+R)(R+\alpha K_P{}^2)}{(K_P+R)^2}$$

Finding R which gives the maximal rate enhancement:

$$\frac{d}{dR}\left(\frac{k^*}{k_{\text{dil}}}\right) = \frac{\alpha K_P{}^3 - \alpha K_P{}^2(R+2) + 2K_PR + K_P - R}{(K_P+R)^3}$$

$$\frac{d}{dR}\left(\frac{k^*}{k}\right) = 0 \;\Leftrightarrow\; K_P{}^3 - \alpha K_P{}^2(R+2) + 2K_PR + K_P - R = 0$$

2nd order $A + B \rightarrow C$, with altered reaction rate constant in the coacervate phase

$$\alpha = \frac{k_{\text{coac}}}{k_{\text{dil}}}$$

$$r_s = k_{\text{coac}} \frac{1}{1+R} [A]_{\text{coac}} [B]_{\text{coac}} + k_{\text{dil}} \frac{R}{1+R} [A]_{\text{dil}} [B]_{\text{dil}}$$

$$r_s = \alpha k_{\text{dil}} \frac{1}{1+R} \cdot \frac{K_{P,A}(1+R)}{K_{P,A}+R} \cdot \frac{K_{P,B}(1+R)}{K_{P,B}+R} [A]_{\text{tot}} [B]_{\text{tot}} + k_{\text{dil}} \frac{R}{1+R} \cdot \frac{1+R}{K_{P,A}+R} \cdot \frac{1+R}{K_{P,B}+R} [A]_{\text{tot}} [B]_{\text{tot}}$$

Assuming that the rate constant in the dilute phase is the same as in the homogeneous system:

$$r_h = k_{\text{dil}} [A]_{\text{tot}} [B]_{\text{tot}}$$

Ratio of the apparent phase-separated and homogenous rate constants:

$$\frac{k^*}{k_{\text{dil}}} = \frac{1+R}{(K_{P,A}+R)(K_{P,B}+R)} (\alpha K_{P,A} K_{P,B} + R)$$

Finding R which gives the maximal rate enhancement:

$$\frac{d}{dR}\left(\frac{k^*}{k_{\text{dil}}}\right) = \frac{R^2(-\alpha K_{P,A} K_{P,B} + K_{P,A} + K_{P,B} - 1) + K_{P,A} K_{P,B}[-2(x-1)R + K_{P,A} K_{P,B} - \alpha K_{P,A} - \alpha K_{P,B} + 1]}{(K_{P,A}+R)^2 (K_{P,A}+R)^2}$$

$$\frac{d}{dR}\left(\frac{k^*}{k}\right) = 0 \Leftrightarrow R^2(-\alpha K_{P,A} K_{P,B} + K_{P,A} + K_{P,B} - 1) + K_{P,A} K_{P,B}[-2(\alpha-1)R + K_{P,A} K_{P,B} - \alpha K_{P,A} - \alpha K_{P,B} + 1] = 0$$

3rd order $A + A + A \rightarrow C$

$$[A]_{\text{coac}} = \frac{K_P(1+R)}{R+K_P} [A]_{\text{tot}}$$

$$[A]_{\text{dil}} = \frac{1+R}{R+K_P} [A]_{\text{tot}}$$

Reaction rate in a phase-separated system (r_s) and homogenous system (r_h):

$$r_s = k\frac{1}{1+R}[A]_{\text{coac}}{}^3 + \text{k}\frac{R}{1+R}[A]_{\text{dil}}{}^3$$

$$r_s = k\frac{1}{1+R}\cdot\frac{(1+R)^2}{(K_P+R)^3}[A]_{\text{tot}}{}^3\left(K_P{}^3+R\right)$$

$$r_h = k[A]_{\text{tot}}{}^3$$

Ratio of the apparent phase-separated and homogenous rate constants:

$$\frac{k^*}{k} = \frac{1}{1+R}\cdot\frac{(1+R)^2}{(K_P+R)^3}\left(K_P{}^3+R\right)$$

Finding R which gives the maximal rate enhancement:

$$\frac{d}{dR}\left(\frac{k^*}{k}\right) = \frac{(K_P-1)^2(R+1)(2K_P{}^2-K_PR+K_P-2R)}{(K_P+R)^4}$$

$$\frac{d}{dR}\left(\frac{k^*}{k}\right) = 0 \;\Leftrightarrow\; 2K_P{}^2-K_PR+K_P-2R = 0; R = \frac{2K_P{}^2+K_P}{K_P+2}$$

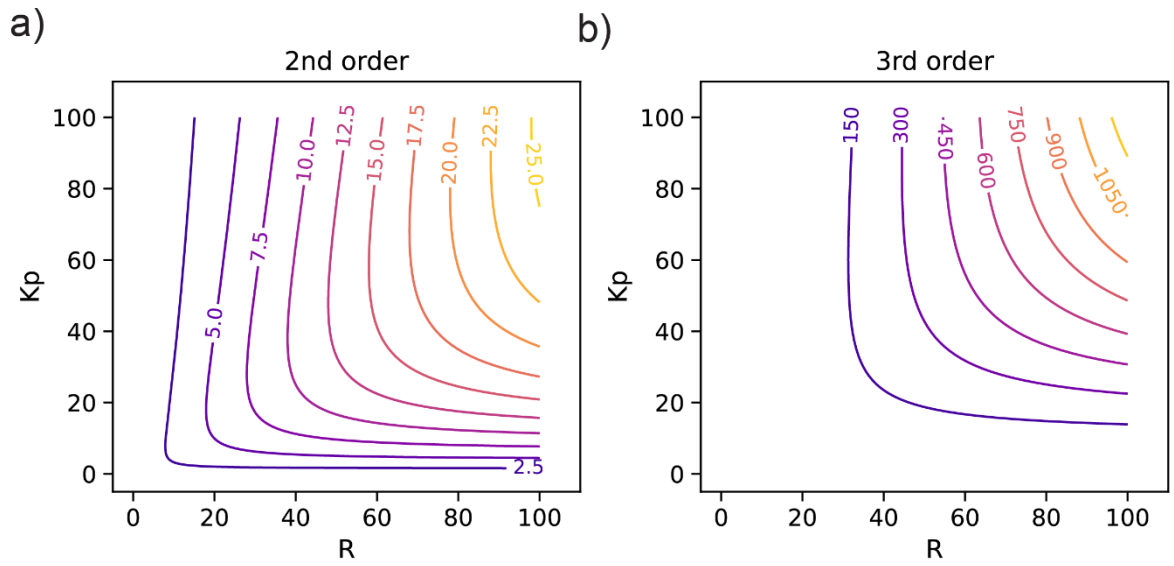

Supplementary Figure 1: Rate enhancement as a function of R and K_P, as determined by numerically solving for $\frac{k^*}{k}$ **(a)** Contour plot showing the regimes of certain rate enhancement factors for second order reactions. **(b)** Contour plot showing the regimes of certain rate enhancement factors for third order reactions.

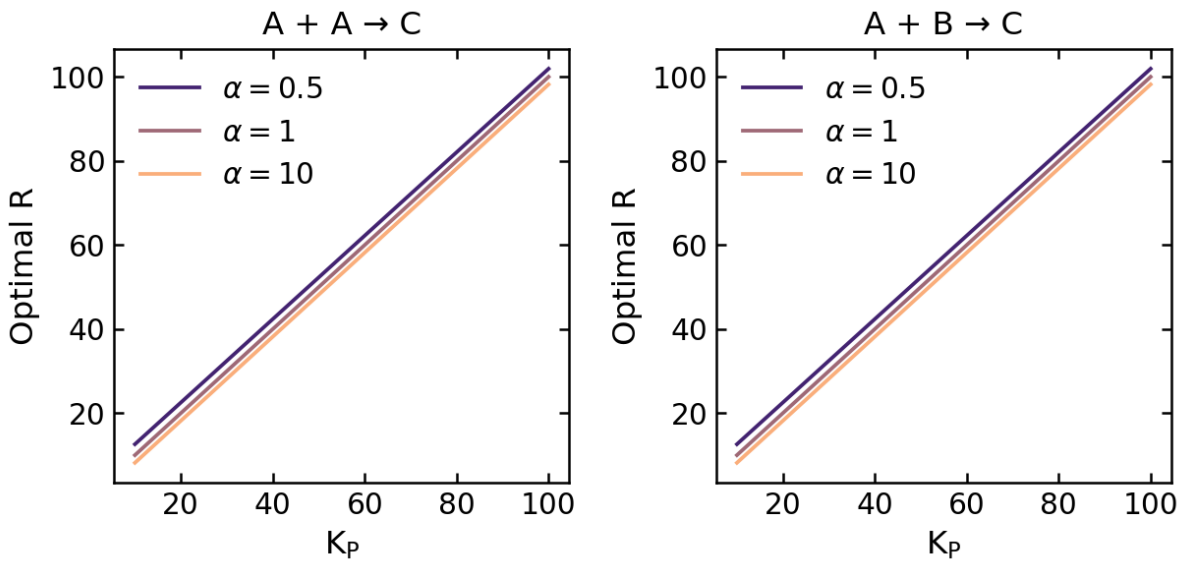

Supplementary Figure 2: The optimal R for a given value of K_P with three rate enhancement factors α within the coacervate phase for bimolecular reactions **(a)** A + A → C and **(b)** A + B → C. For higher α, the optimal R is smaller for the same K_P.

2.2. Supplementary figures for the bimolecular reaction

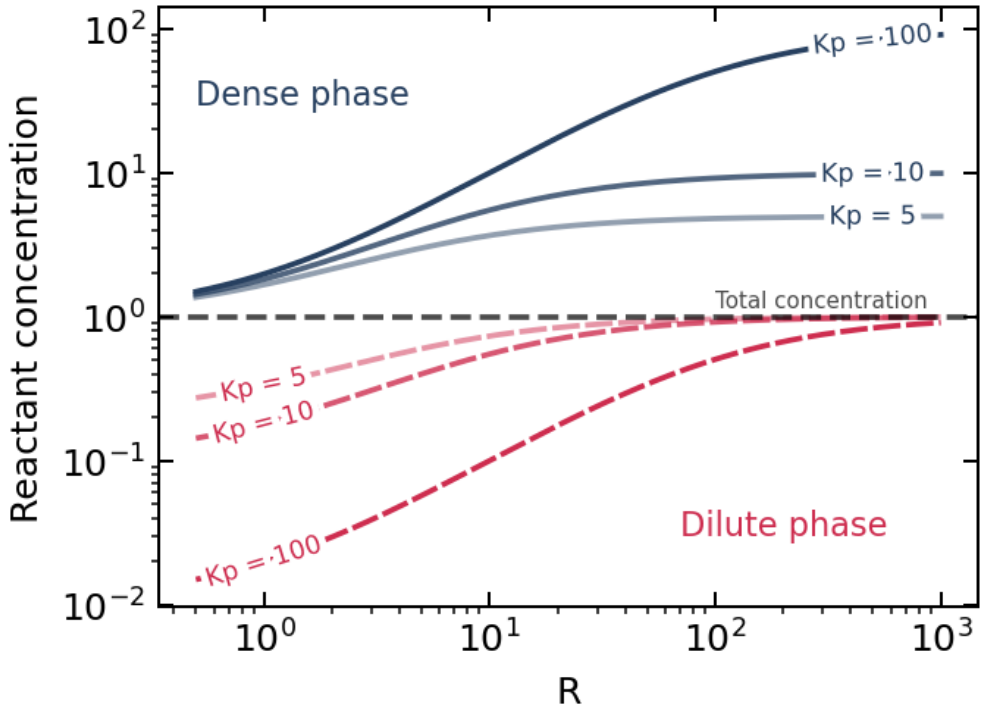

Supplementary Figure 3: Reactant concentration in the dense and dilute phase as a function of R for different K_P's. From the point of maximal rate enhancement $K_P = R$, a decrease in R will result in a lower reactant concentration inside the dense phase.

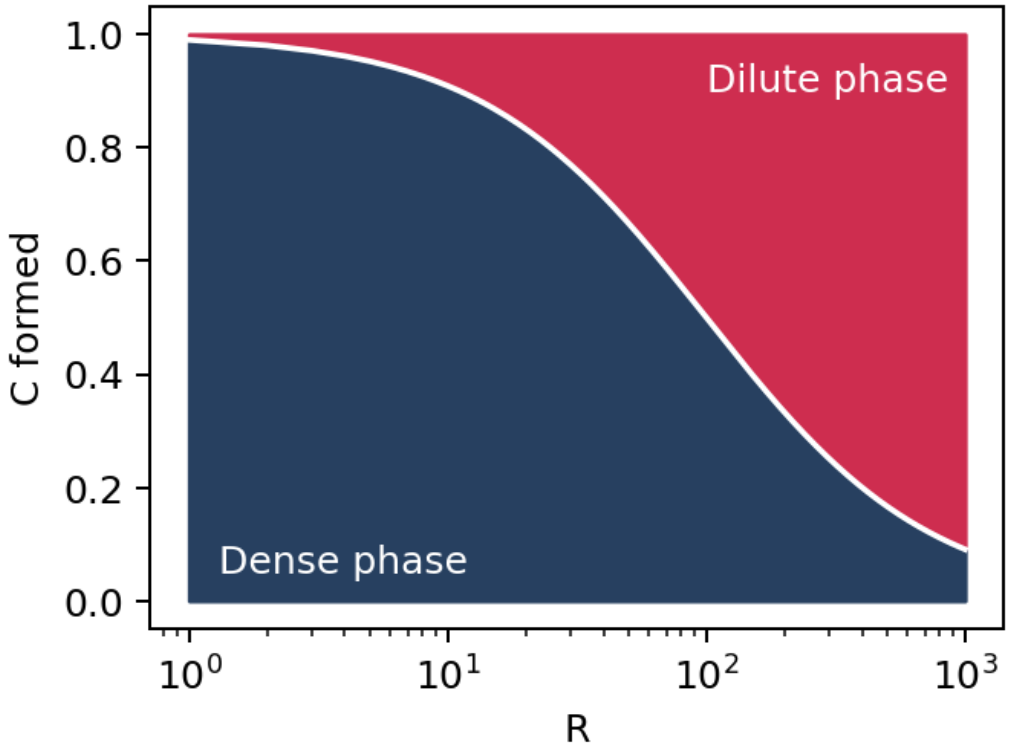

Supplementary Figure 4: Fraction of C formed per phase as a function of R (K_P= 10). The smaller the coacervate (large R), the more C is formed in the dilute phase. At the point of maximum rate enhancement K_P= R = 10, 10x as much C is formed in the dense phase as in the dilute phase.

3. Supplementary results for the polymerization reaction

3.1. Supplementary figures for the polymerization reaction

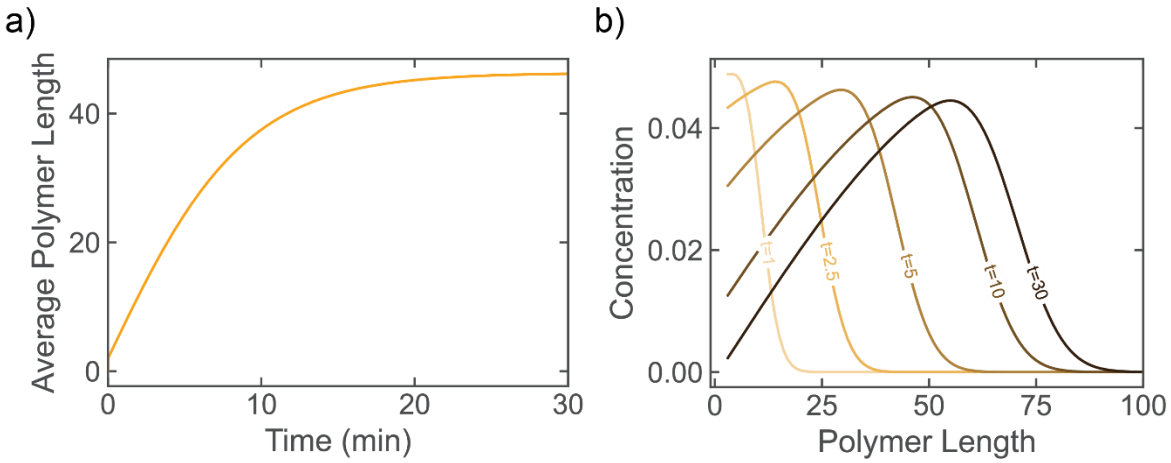

Supplementary Figure 5: Polymerization in a single-phase system ($k_{initiation}$ = 5*10^{-5}; $k_{propagation}$ = 0.1). **(a)** Average polymer length increases over time until a maximum is reached when monomer runs out. **(b)** The distribution of polymer lengths shifts over the course of the reaction.

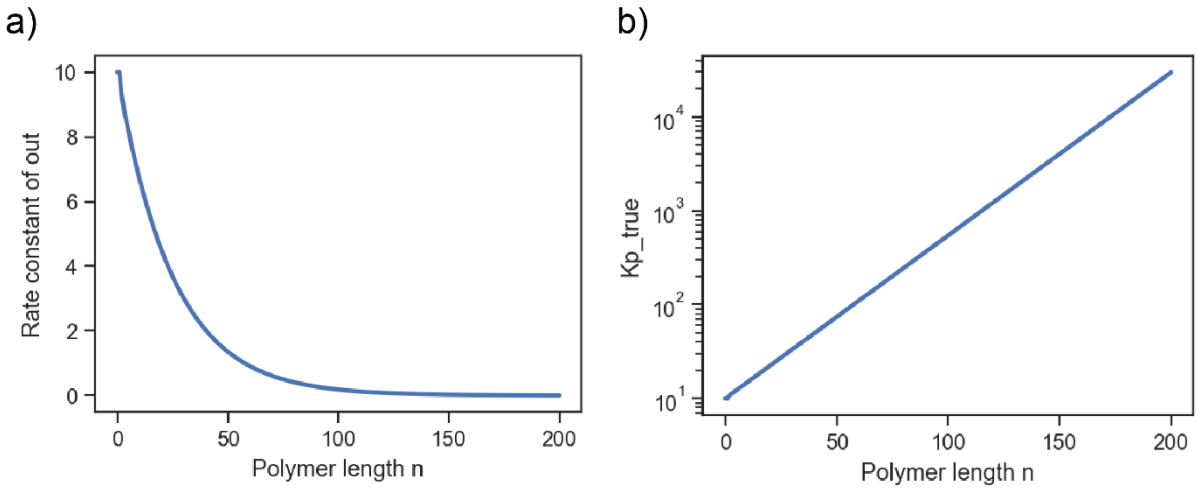

Supplementary Figure 6: The rate constant for outflow from the coacervate is modeled to be lower for longer polymers, according to $k_{\mathrm{cond}\rightarrow\mathrm{dil}} = \mathrm{k}_{\mathrm{out,monomer}} * \mathrm{e}^{-\mathrm{n}\cdot 1/25}$. **(a)** Rate constant for outflow from the coacervate ($\mathrm{k}_{\mathrm{out}} = \mathrm{k}_{\mathrm{cond}\rightarrow\mathrm{dil}}$) for different polymer lengths. **(b)** Because $K_P = \frac{k_{\mathrm{dil}\rightarrow\mathrm{cond}}}{k_{\mathrm{cond}\rightarrow\mathrm{dil}}}$, the effective K_P increases for longer coacervates.

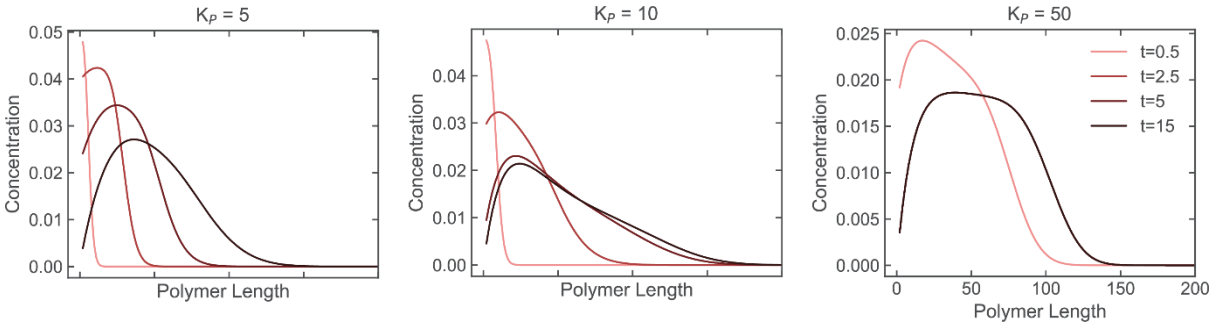

Supplementary Figure 7: Distributions of polymer length over time for different monomer K_P's. The distribution becomes broader for larger K_P.

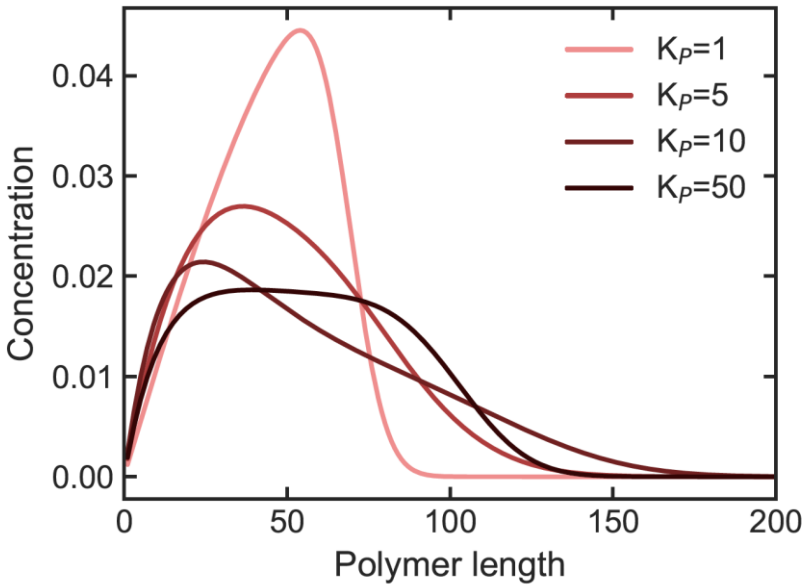

Supplementary Figure 8: Distributions of final polymer length for different monomer K_P's. The distribution becomes broader for larger K_P.

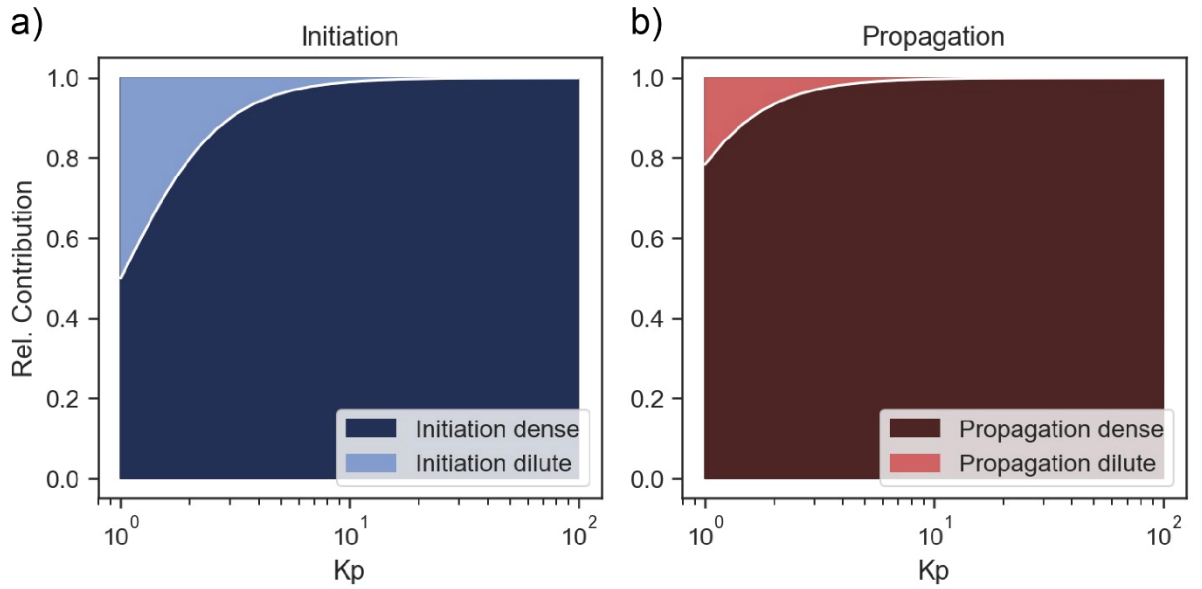

Supplementary Figure 9: Contribution of the dilute and dense phase to the initiation and propagation reaction for different K_P's. At high K_P both reactions take place almost exclusively in the dense phase, but at low K_P the contribution of the dense phase to the propagation reaction is larger than the contribution of the dense phase to initiation.

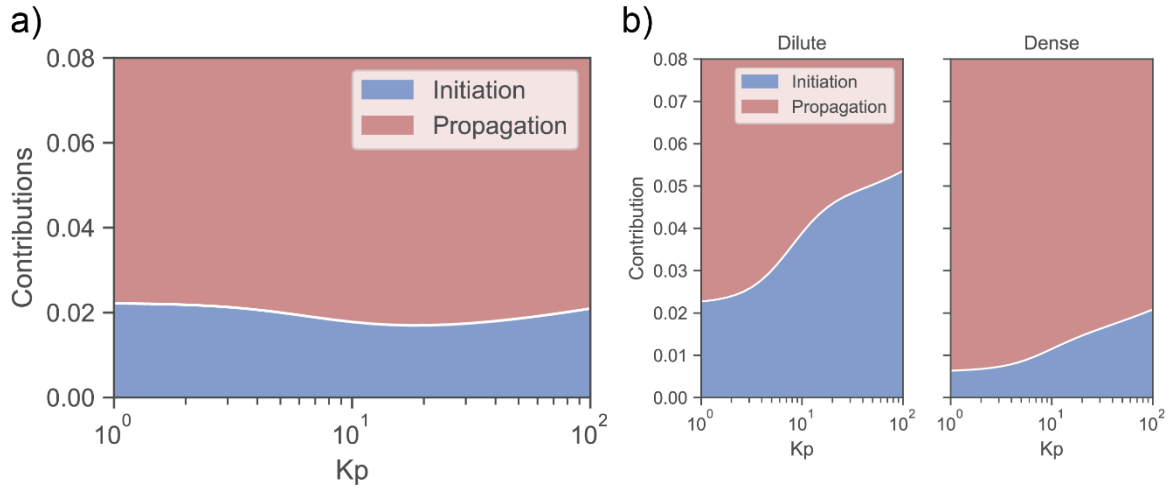

Supplementary Figure 10: Contribution of the initiation and propagation reaction **(a)** for the total reaction and **(b)** per phase. The dip in the contribution of initiation to the total sample coincides with the maximum in average polymer length. For both the dense and dilute phase the contribution of the initiation reaction increases for larger K_P. For the dense phase this is because the partitioning of the monomer increases. For the dilute phase both the monomer and polymers are depleted from the phase at larger K_P, but the polymers are depleted to a larger extent, leading to an increase in the relative contribution of the initiation reaction. Note that the y-axis is cropped to show the contribution of the initiation reaction more clearly.

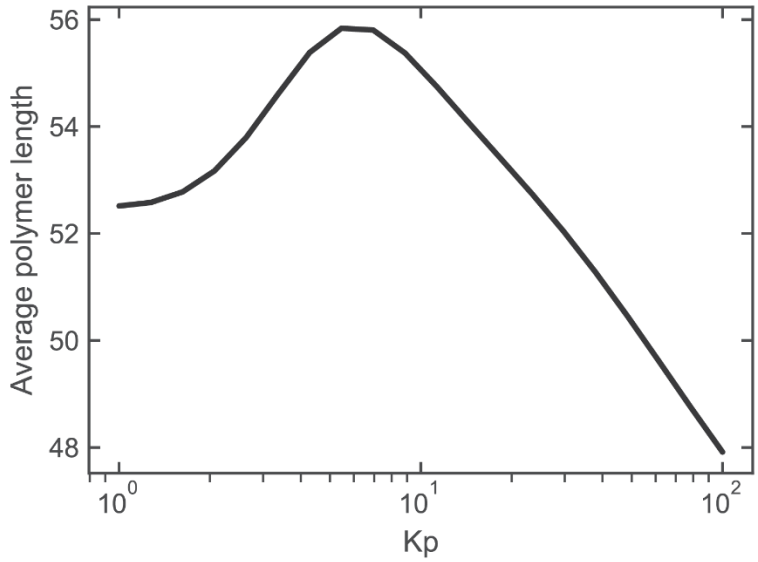

Supplementary Figure 11: Weight average polymer length for different monomer K_P's.

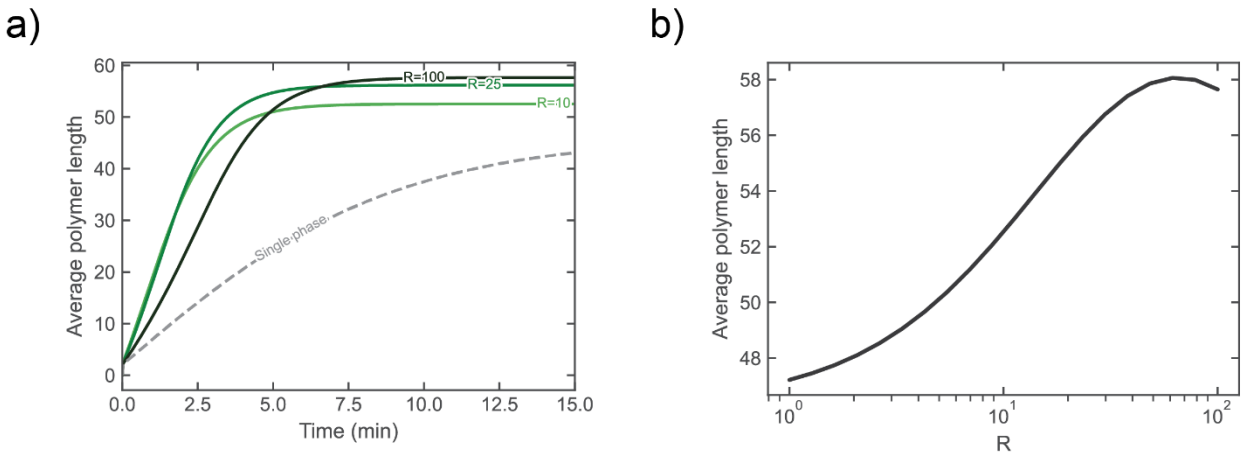

Supplementary Figure 12: Evolution of average polymer length over time for different R (K_P = 10). **(a)** For smaller coacervate volumes (larger R), a higher final polymer length is obtained, while for larger coacervate volumes (smaller R), long polymers are formed more rapidly. **(b)** The average polymer length increases as a function of R until a maximum around R = 70.

4. Supplementary results for the self-replication

4.1. Supplementary Information for the self-replication reaction

Supplementary Table 5: Literature values for the ratio of the autocatalytic rate constant and bimolecular (non-autocatalytic) rate constant. For literature, the values are reported according to the formula $\left[\frac{d[T]}{dt}\right]_{\text{initial}} = k_{\text{autocatalytic}}[T]_o{}^{p} + k_{\text{bimolecular}}$, so $k_{\text{autocatalytic}}$ represents the whole autocatalytic cycle. In our model $k_{\text{autocatalytic}}$ is only for the ligation step. Considering that the whole autocatalytic cycle included the unfavorable dissociation of the TT duplex, the rate constant of the ligation step in the literature examples is likely higher than $k_{\text{autocatalytic}}$.

Paper	$k_{autocatalytic}$	$k_{bimolecular}$	Fold-enhancement
Von Kiedrowski Angewandte 1986[1]	$9.48 \cdot 10^{-8}$	$3.83 \cdot 10^{-9}$	$2.48 \cdot 10^{1}$
Paul. Joyce PNAS 2002[2]	0.011	$3.30 \cdot 10^{-11}$	$3.33 \cdot 10^{8}$
Lee Nature 1996[3]	29.4	0.063	$4.67 \cdot 10^{2}$
Issac JACS 2002[4]	50.6	$5.04 \cdot 10^{-4}$	$1.00 \cdot 10^{5}$
Our model	1.2	$7.30 \cdot 10^{-2}$	$1.64 \cdot 10^{1}$
Our model (100x slower)	1.2	$7.30 \cdot 10^{-4}$	$1.64 \cdot 10^{3}$

4.2. Supplementary figures for the self-replication reaction

To better understand the results of the self-replication in a two-phase system. we investigated the system from Figure 3 in a single phase (Supplementary Figure 13-14) and in a two-phase system, but in absence of transfer of different reaction components (Supplementary Figure 15-25).

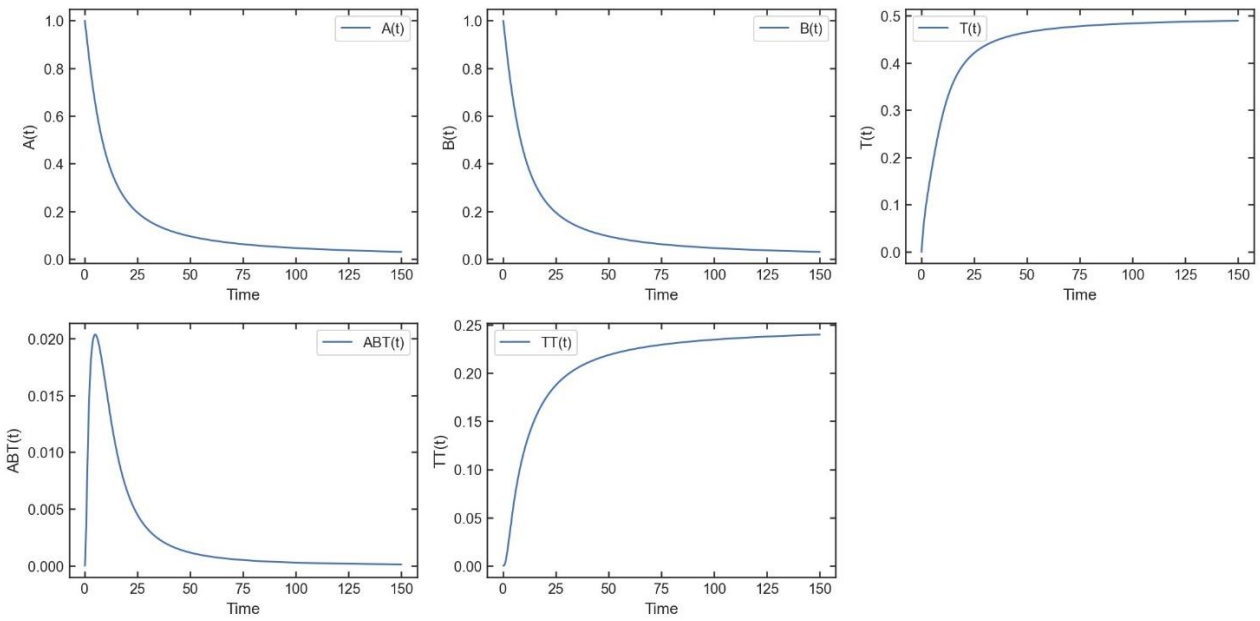

Supplementary Figure 13: Amount of A, B, T, ABT and TT present over the course of the reaction in a single-phase system.

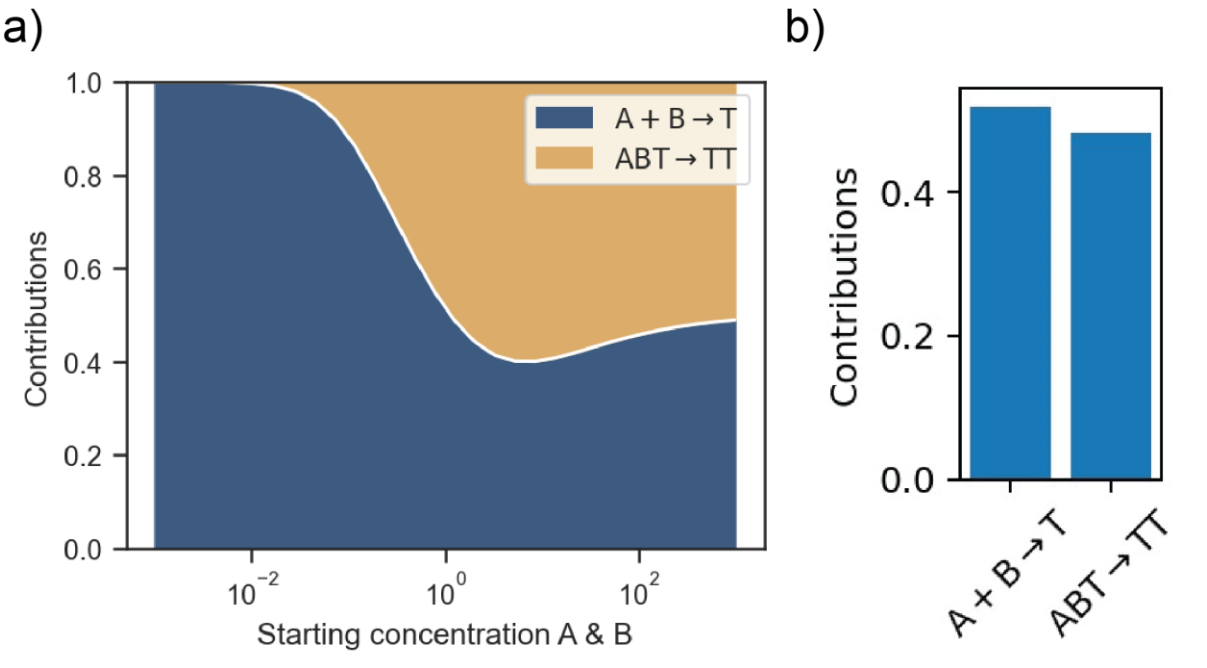

Supplementary Figure 14: Self-replication reaction in a single-phase system **(a)** with varying starting concentrations. Similarly to the two-phase system. a maximum in contribution of the autocatalytic pathway is observed. **(b)** Relative contribution of the bimolecular and autocatalytic ligation at the concentrations used in our simulation.

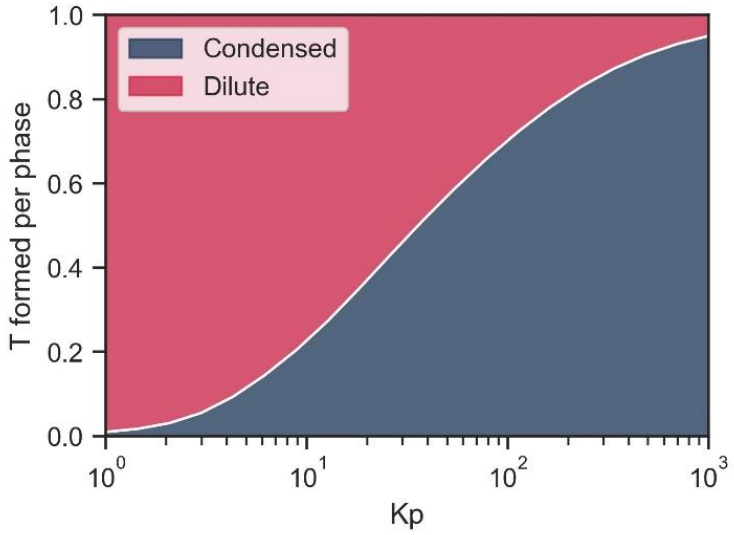

Supplementary Figure 15: Amount of T formed per phase (R = 100). The transition from the majority of T being formed in the dilute phase to the majority of T being formed in the dense phase is around K_P = 30.

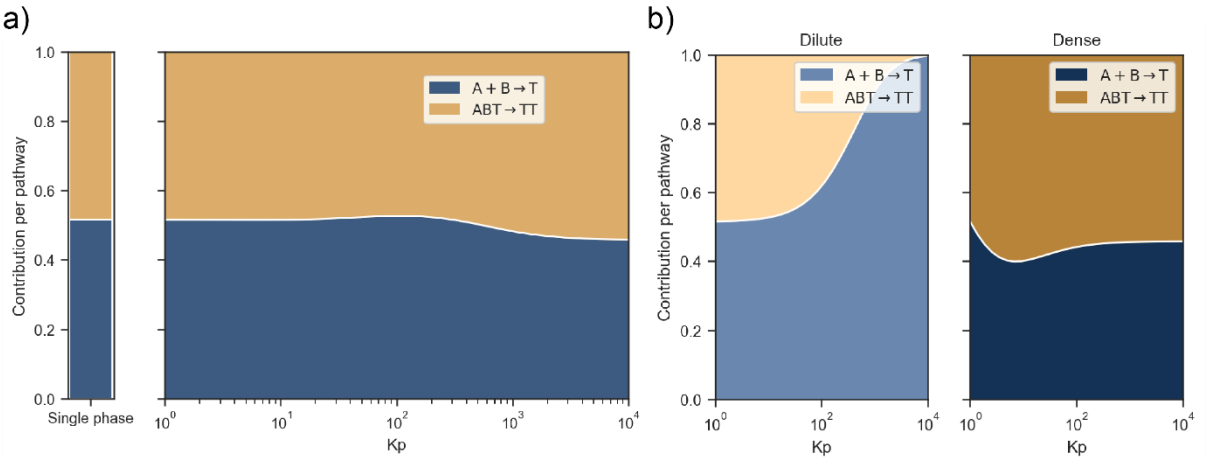

Supplementary Figure 16: Self-replication reaction in a two-phase system in absence of transfer of any component (K_P = 10. R = 100). **(a)** Contribution of the autocatalytic and bimolecular pathway on the total system. **(b)** Contribution of the autocatalytic and bimolecular pathway per phase. Without exchange between the phases. The contributions in the dilute phase follows the same trend as in a single-phase system (Supplementary Figure 4) upon going from intermediate to low concentrations. while the contributions in the dense phase follow the single-phase trend for going from intermediate to high concentrations.

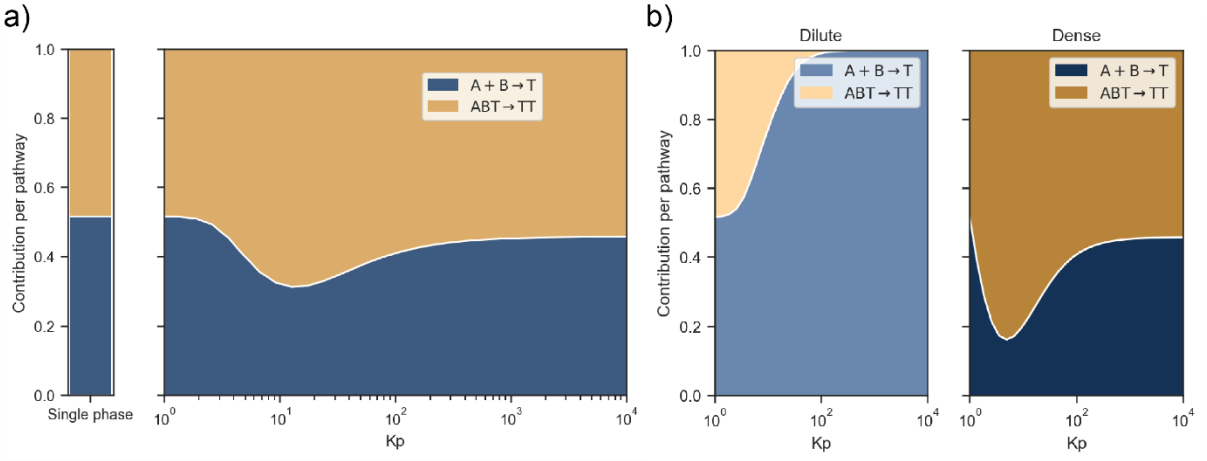

Supplementary Figure 17: Self-replication reaction in a two-phase system in absence of transfer of ABT. TT and T. **(a)** Contribution of the autocatalytic and bimolecular pathway on the total system. **(b)** Contribution of the autocatalytic and bimolecular pathway per phase. In the dense and dilute phase. The same trend is observed as in absence of transfer of all components (Supplementary Figure 6), indicating that either ABT. TT or T transfer is critical to get the outcome in Figure 3d.

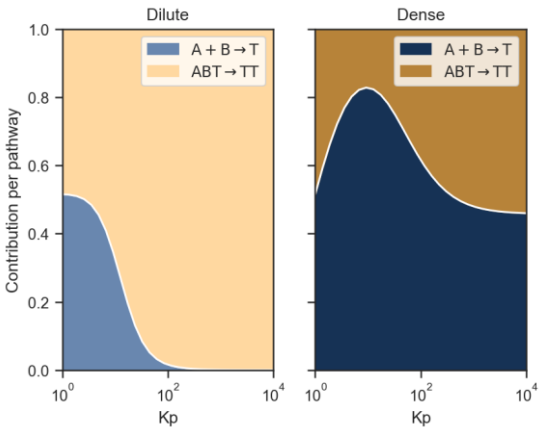

Supplementary Figure 18: Self-replication reaction in a two-phase system in absence of transfer of T. In the dense and dilute phase. The same trend is observed as in the case with of transfer of all components, indicating that T is not critical to get the outcome in Figure 3d.

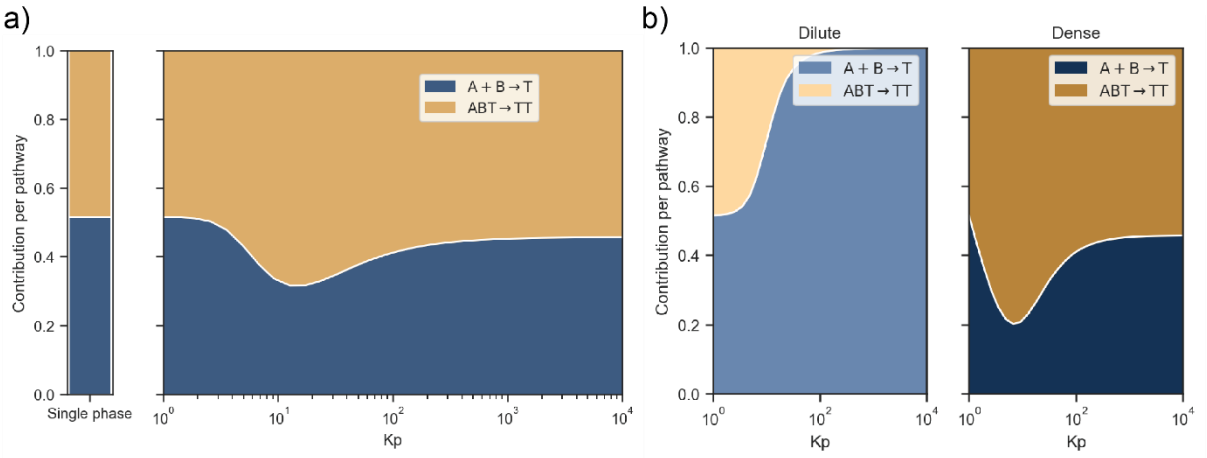

Supplementary Figure 19: Self-replication reaction in a two-phase system in absence of transfer of ABT and TT. **(a)** Contribution of the autocatalytic and bimolecular pathway on the total system. **(b)** Contribution of the autocatalytic and bimolecular pathway per phase. In the dense and dilute phase. The same trend is observed as in absence of transfer of all components (Supplementary Figure 6), indicating that either ABT or TT transfer is critical to get the outcome in Figure 3d.

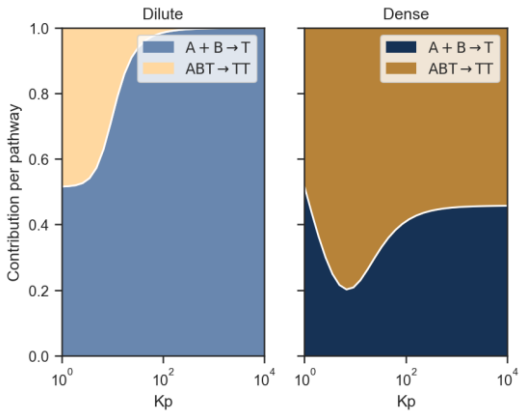

Supplementary Figure 20: Self-replication reaction in a two-phase system in absence of transfer of ABT. In the dense and dilute phase. The same trend is observed as in absence of transfer of all components (Supplementary Figure 6), indicating that ABT transfer is critical to get the outcome in Figure 3d.

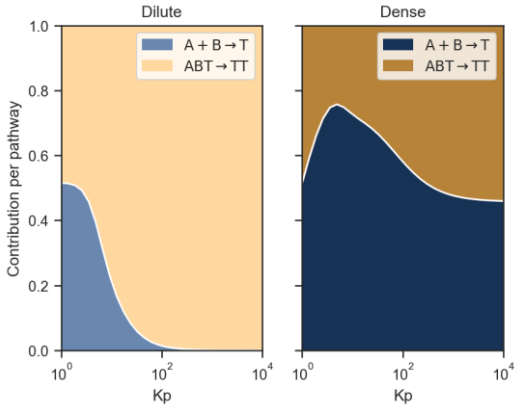

Supplementary Figure 21: Self-replication reaction in a two-phase system in absence of transfer of TT. In the dense and dilute phase. The same trend is observed as in the case with of transfer of all components, indicating that TT is not critical to get the outcome in Figure 3d.

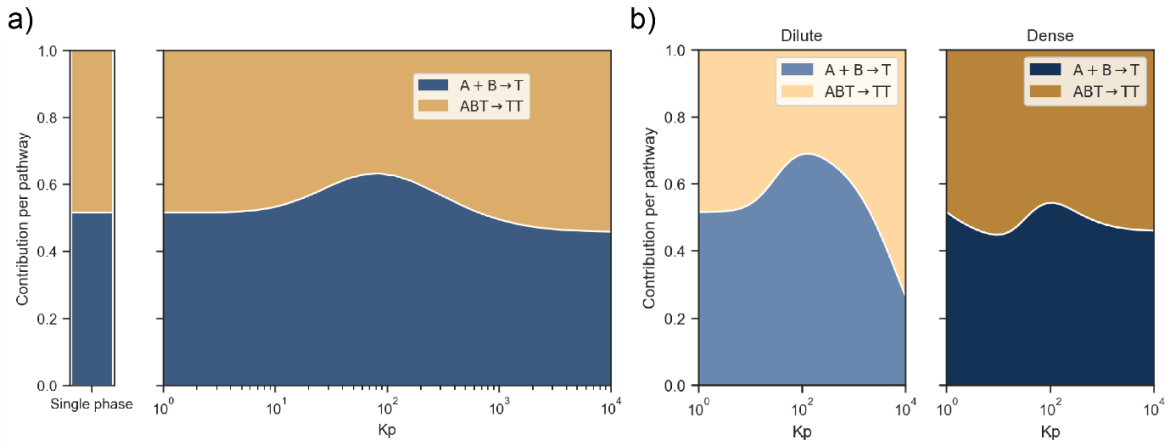

Supplementary Figure 22: Self-replication reaction in a two-phase system in absence of transfer of A and B. **(a)** Contribution of the autocatalytic and bimolecular pathway on the total system. **(b)** Contribution of the autocatalytic and bimolecular pathway per phase. Absence of A and B transfer completely changes the profile of distributions of the reactions. For low to moderate K_P the profile is similar to the profile in absence of any transfer. For moderate to high K_P the distributions in the dense and dilute phase more closely resemble the distributions in presence of transfer of all species.

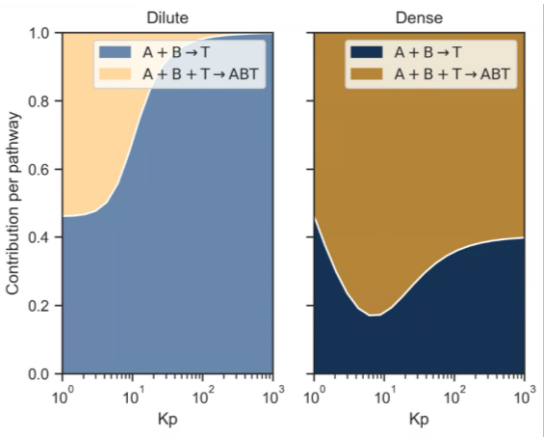

Supplementary Figure 23: Formation of ABT complex per phase for the self-replication reaction. The termolecular reaction to form complex ABT is unfavorable in dilute conditions and takes place preferentially in the more concentrated dense phase, while in the dilute phase the bimolecular reaction between A and B is favored over the termolecular reaction to form complex ABT.

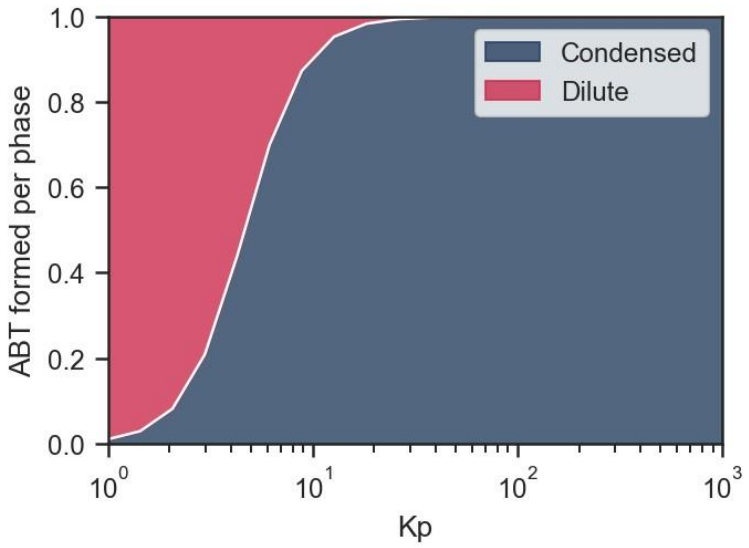

Supplementary Figure 24: Amount of ABT formed per phase via A + B + T → ABT. The formation of ABT takes place mostly in the dense phase, already for lower values of K_P. The distribution shifted to the left compared to the total reaction in Supplementary Figure 5.

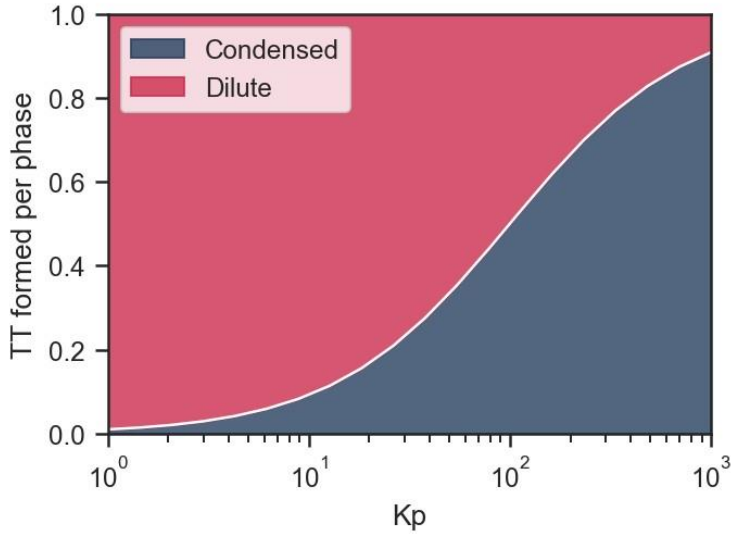

Supplementary Figure 25: Amount of TT formed per phase via ABT → TT. The formation of TT takes place mostly in the dilute phase, even for higher values of K_P. The distribution is shifted to the right compared to the total reaction in Supplementary Figure 5.

4.3. Supplementary figures for self-replication with lower rate for the bimolecular reaction

To investigate the robustness of the simulations. and explore a $\frac{k_{\text{autocatalytic ligation}}}{k_{\text{bimolecular}}}$ ratio that better resembles the higher range of values found in literature (Supplementary Table 5). we also investigated the reaction with a 100x slower rate of the bimolecular reaction. The results are represented in Supplementary Figure 26-30.

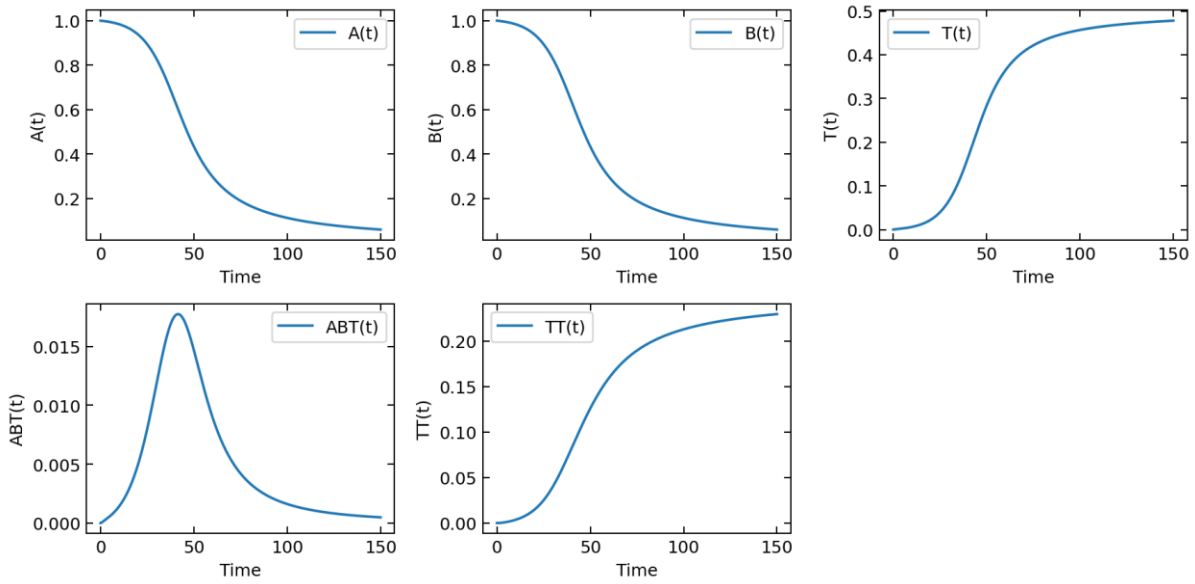

Supplementary Figure 26: Amount of A, B, T, ABT and TT present over the course of the reaction for a slow bimolecular reaction in a single-phase system.

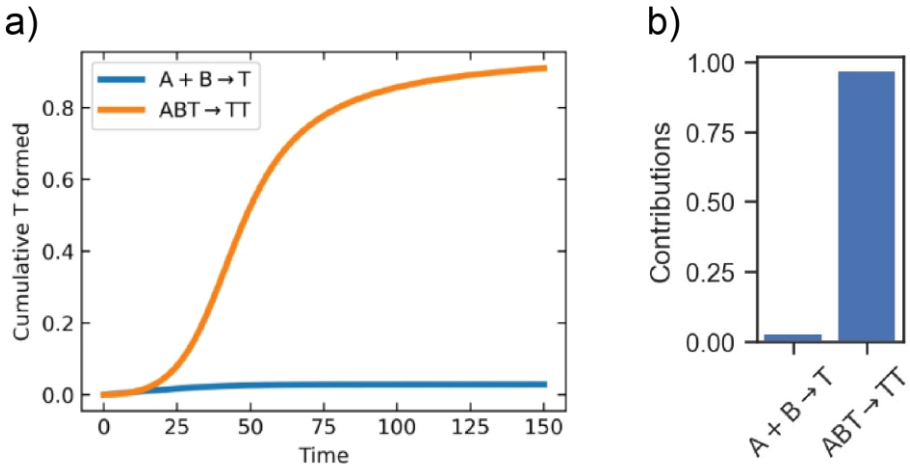

Supplementary Figure 27: Contribution of the bimolecular and autocatalytic reaction pathway in T formation for the slow bimolecular reaction in a single-phase system. **(a)** Cumulative amount of T formed via the bimolecular (A + B → T) and autocatalytic (ABT → TT) pathway. **(b)** Fraction of contributions of both pathways to the total system.

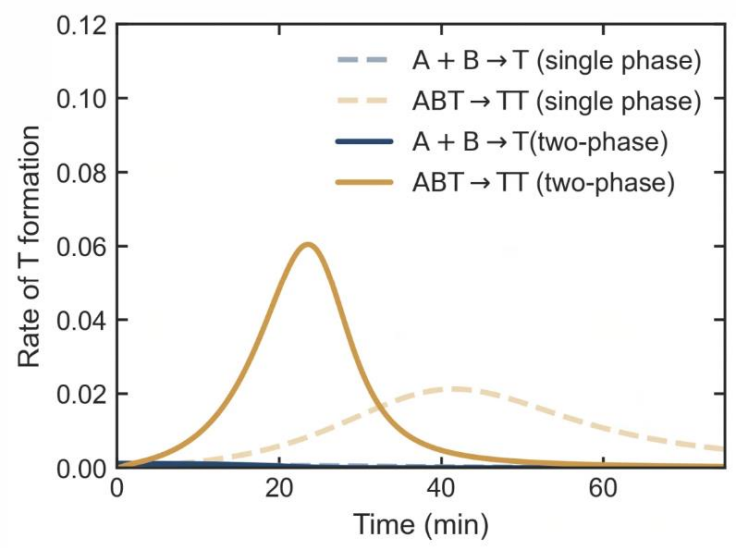

Supplementary Figure 28: A comparison between the T formed through the autocatalytic (ABT → TT) and non-autocatalytic pathway (A + B → T) in a single-phase and in a two-phase system (K_P = 10. R = 100) for a slow bimolecular reaction. For a slow bimolecular reaction, the autocatalytic pathway dominates at every timepoint after the first minute. and the maximum rate of T formation is obtained at a later time than for a faster bimolecular reaction due to a longer lag time of the system.

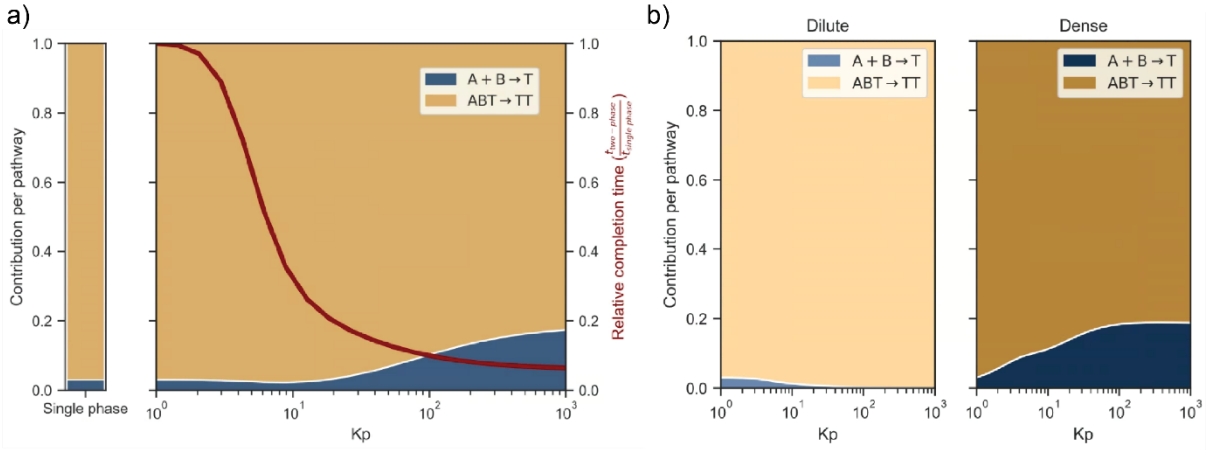

Supplementary Figure 29: Self-replication in a two-phase system with a slow rate of the bimolecular reaction. **(a)** Contribution of the autocatalytic and bimolecular pathway on the total system. and relative completion time compared to a single-phase system. **(b)** Contribution of the autocatalytic and bimolecular pathway per phase. The system with a slow rate of the bimolecular reaction shows similar behavior as a system with larger rate of the bimolecular reaction (Figure 3c & d). At low K_P the total system is dominated by the reaction in the dense phase. while for larger K_P the dense phase reaction dominates. Similar to Figure 3c there is a (shallow) maximum in the contribution of the autocatalytic reaction. and for high K_P the contribution of the bimolecular reaction increases. Contrary to Figure 3c for a slow bimolecular reaction the system does not reach equal contribution of the dense and dilute phase for high K_P.

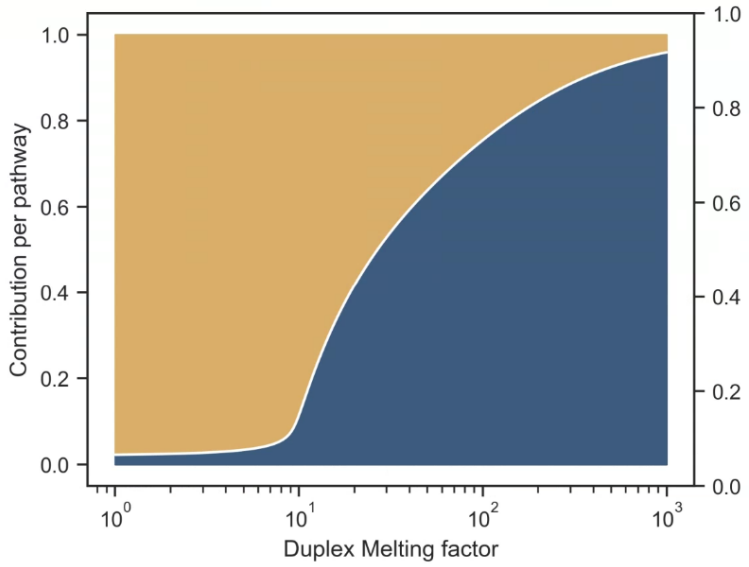

Supplementary Figure 30: An increased duplex melting within the dense phase leads to an increase in the non-autocatalytic pathway, also for the slower bimolecular reaction. with a sharper transition than for the faster bimolecular reaction in Figure 3e (K_P = 10. R = 100).

5. Supplementary results for the oscillatory reaction network

5.1. Supplementary figures for the oscillatory reaction network

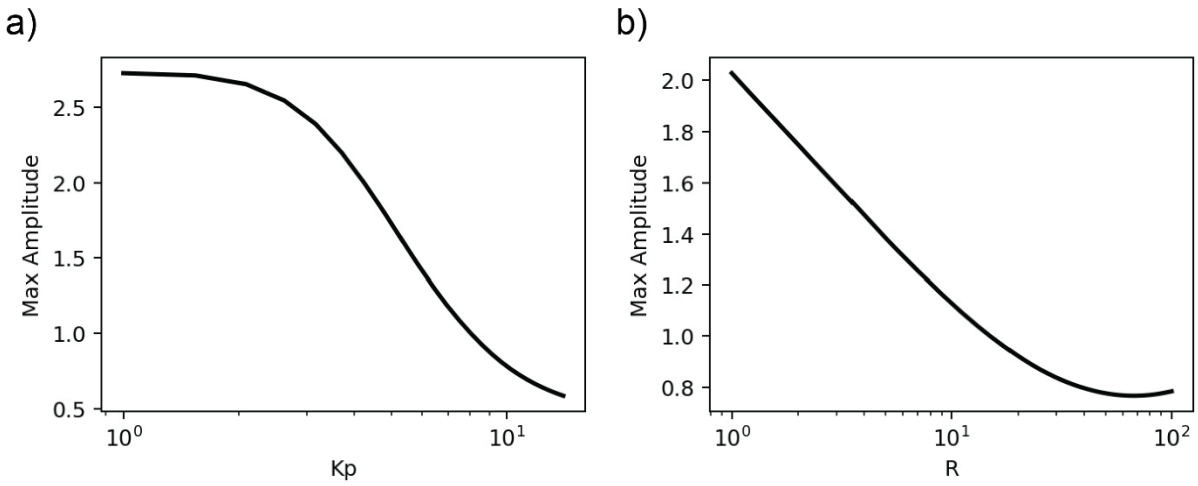

Supplementary Figure 31: Change in the maximum amplitude of oscillations between 5 and 50 minutes as a function of **(a)** K_P (R = 100) and **(b)** R (K_P = 10). The maximum amplitude decreases both as a function of K_P and as a function of R. For very large R the maximum amplitude increases slightly again.

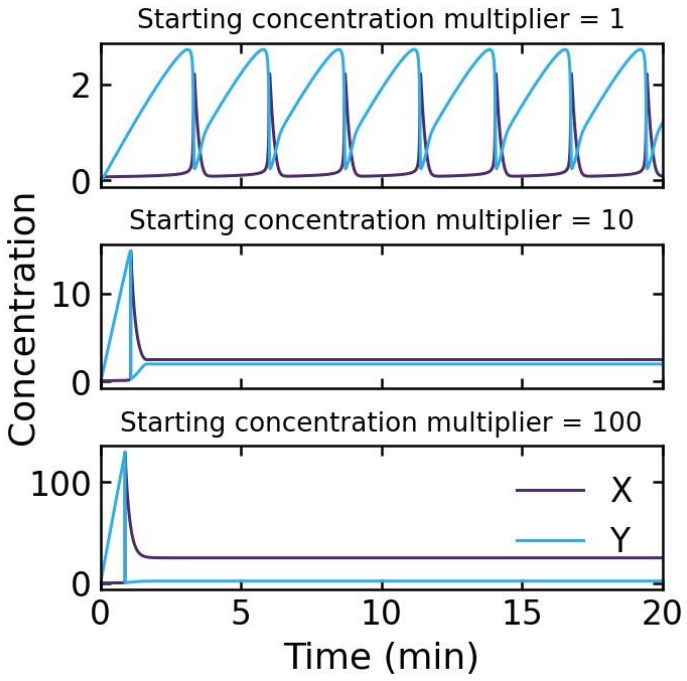

Supplementary Figure 32: Oscillations at different concentrations in a single-phase system.

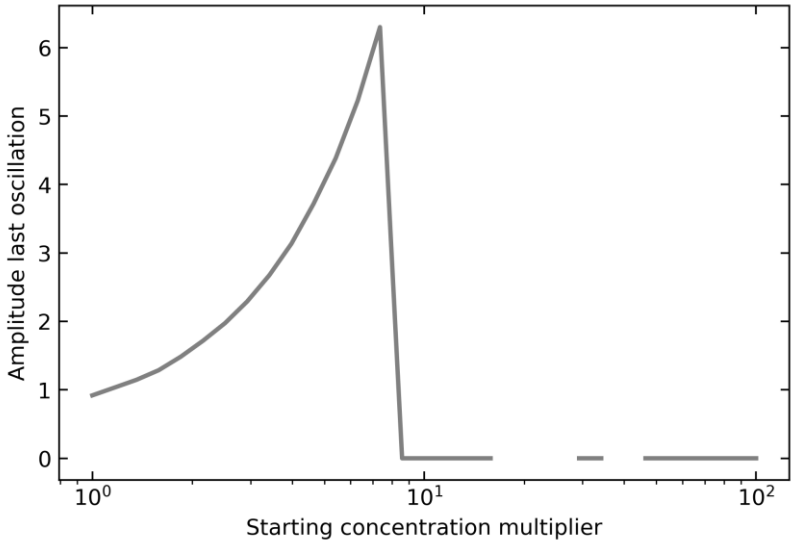

Supplementary Figure 33: Amplitude of the final oscillation in the time simulated for the network in a single-phase system at different concentrations. Sustained oscillations disappear when the system becomes about 8x as concentrated as the initial concentration. The remaining oscillations after the peak have a low amplitude and are assumed to be an artifact of the numerical solver.

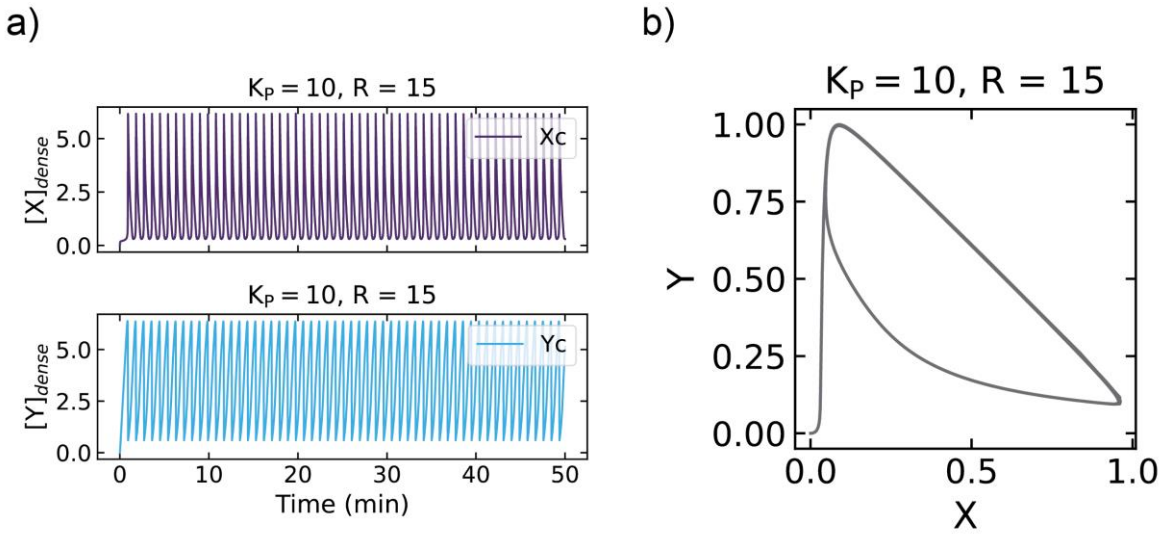

Supplementary Figure 34: Oscillatory reaction network for K_P = 10. R = 15. **(a)** Oscillations in X and Y in the dense phase. **(b)** The phase plot shows that the system enters the limit cycle immediately after initiation.

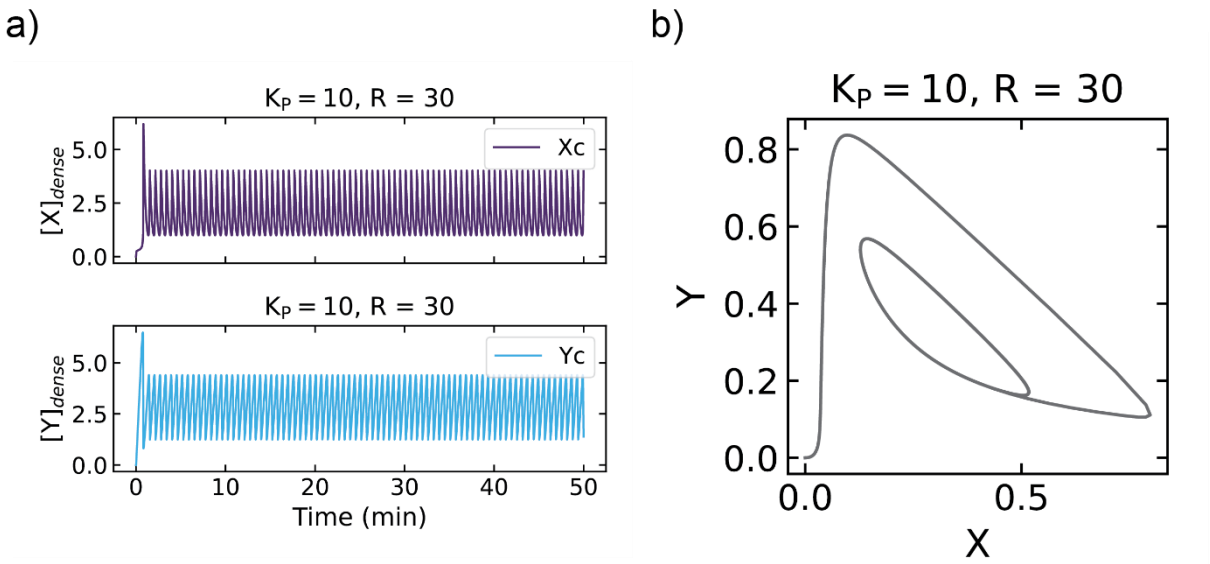

Supplementary Figure 35: Oscillatory reaction network for K_P = 10. R = 30. **(a)** Oscillations in X and Y in the dense phase. Amplitude is lower than for R = 30 (Supplementary Figure 20). while the period is shorter. **(b)** The phase plot shows that the system enters the limit cycle only after an initial larger cycle.

6. Supplementary references

(1) von Kiedrowski. G. A Self-Replicating Hexadeoxynucleotide. *Angew. Chemie Int. Ed. English* **1986**. *25* (10). 932–935. https://doi.org/10.1002/anie.198609322.

(2) Paul. N.; Joyce. G. F. A Self-Replicating Ligase Ribozyme. *Proc. Natl. Acad. Sci. U. S. A.* **2002**. *99* (20). 12733–12740. https://doi.org/10.1073/pnas.202471099.

(3) Lee. D. H.; Granja. J. R.; Martinez. J. A.; Severin. K.; Ghadiri. M. R. A Self-Replicating Peptide. *Nature* **1996**. *382* (6591). 525–528. https://doi.org/10.1038/382525a0.

(4) Issac. R.; Chmielewski. J. Approaching Exponential Growth with a Self-Replicating Peptide. *J. Am. Chem. Soc.* **2002**. *124* (24). 6808–6809. https://doi.org/10.1021/ja026024i.